Escola Tècnica Superior d'Enginyeries Industrial i Aeronàutica de Terrassa

UNIVERSITAT POLITÈCNICA DE CATALUNYA

BACHELOR'S DEGREE:

AEROSPACE VEHICLES ENGINEERING

AUTHOR:

JUAN HITA GARCÍA

TITLE:

TECHNICAL STUDY OF A MODEL AIRPLANE FOR THE AIR CARGO CHALLENGE

DIRECTOR:

DANIEL GARCÍA ALMIÑANA

COURSE:

2014-2015 Q2

CONTENT OF THIS DOCUMENT:

REPORT

In memory of my father, whose sacrifice and dedication inspired me through this trip. Dedicated to my family and friends, for all the love and support given.

SUMMARY OF CONTENTS

LIST OF FIGURES

LIST OF TABLES

LIST OF SYMBOLS

Symbol	Units	Description
α	rad	Alpha/Angle of attack
β	rad	Beam section rotation
γ	rad	Climb rate angle
δ	rad	Flap deflection
μ	rad	Ground friction coefficient
π	rad	Throttle parameter
ρ	kg/m^3	Density
τ	Pa	Shear force
σ	Pa	Stress
AR	-	Aspect Ratio
b	m	Wing span
c	m	Chord
E	Pa	Young modulus
e	-	Planform aerodynamic efficiency
g	m/s^2	Gravity
I	m^4	Moment of inertia
M	Nm	Moment
m	kg	Mass
n	-	Normal direction, Load factor
σ	Pa	Stress
p_∞	Pa	Pressure in the freestream
Pa	W	Power available
Pn	W	Power necessary
Q	N	Shear force in a section
q	W	Heat transfer
q	N/m	Shear flow
R’	N	Reaction on body in flow
t	m	Wall thickness
u	m/s	Horizontal freestream speed component

$V\infty$	m/s	Freestream speed
W	N	Weight
w	m/s	Induced speed

Acronyms

AoA	Angle of Attack
ACC	Air Cargo Challenge
CAD	Computer Aided Design
CAM	Computer Aided Manufacturing
CFD	Computational Fluid Dynamics
CFRP	Carbon Fiber Reinforced Plastic
FEA	Finite Element Analysis
MTOW	Maximum Take-off Weight
PWM	Pulse-Width Modulation
RANS	Reynolds Averaged Navier-Stokes
UAV	Unmanned Aircraft Vehicle
UPC	Universitat Politècnica de Catalunya

1. AIM

The main goal of this study is to establish a set of guidelines for future members of UPC Venturi on how to design, build and test model airplanes. These methodologies have been applied for the Air Cargo Challenge 2015, an international competition where the team has competed in Stuttgart, Germany. Moreover, several improvements will be proposed as part of this study for future aircrafts.

2. SCOPE

The scope of this study will be divided in three main parts. First of all, chapter 6 will include a generic handbook regarding the technical development of a model airplane considering the following fields of study: conceptual/preliminary design, aerodynamics, propulsion and performance, structural design, materials and CAD/CAM process. The aim of this section is to provide the basic knowledge to a new student to start designing an aircraft, giving an extra emphasis to practical application of contents that are seen during theory lectures. It is not within the scope of this handbook to explain all the conceptual knowledge behind the calculations, but to provide a practical vision of the development of this kind of projects.

Secondly, application of these guidelines for the Air Cargo Challenge 2015 aircraft and the technical results will be detailed and commented in chapter 7. In this section, the contents developed with the collaboration of other members of the team will be mentioned. Afterwards, based on the results of the competition, some improvement proposals and key points to be competitive in the following edition are exposed in chapter 8.

Finally, management issues are detailed from chapter on. This part contains an economic summary, an environmental impact study and a safety considerations list. Moreover, planning of future tasks are detailed.

3. REQUIREMENTS

First of all, to successfully complete the bachelor's degree these two skills must be demonstrated:

- Entrepreneurship and innovation- Level 3: Using knowledge and strategic skills to create and manage projects, applying systematic methodologies to solve complex problems and design and manage innovation in organizations.
- Solvent use of information resources- Level 3: Planning and using all the information necessary to complete an academic task.

In relation to the requirements to meet during the design phase, the regulations statements to participate in the Air Cargo Challenge 2015 are listed below.

PROPULSION REQUIREMENTS:

- Maximum take-off distance 60m.
- Motor must be a single unmodified AXI Gold 2826/10.
- Lithium based batteries up to 3 cells in series. Maximum continuous discharge capacity must be at least 45A.
- Independent RX battery 600mAh must be included.
- Propeller(s) must be unmodified APC 13x7" Sport.
- Transmission relationship between motor and propeller must be 1:1.

AIRCRAFT DIMENSIONS:

- Assembled plane must fit in a 2,5 x 2,5 m^2 square standing on its landing gear. Aircraft parts must fit in a transportation box which cannot exceed 1100 x 500 x400 mm^3.
- Cargo bay dimensions are 160 x 80 x 80 mm^3.

PILOTING:

- Control assistance systems such as gyroscopes are forbidden.

IDENTIFICATION:

- Wings and fuselage must be clearly identified with the number of the team with figures of at least 10cm height –both sides on fuselage and both bottom and top on wings–.
- University name should be visible on wings or fuselage.

The flight pattern consists of taking-off from a 60m runway, turning back and flying as many 100m flight legs as possible (it is allowed to start turning before the 100m mark, but if the plane does not reach the position it will not be a valid leg to increase the score).

Finally, the score is provided with the following formula:

$$Flight\ Score = (2 \cdot Payload)(Flight\ legs + 3) \quad \textit{(Eq. 1)}$$

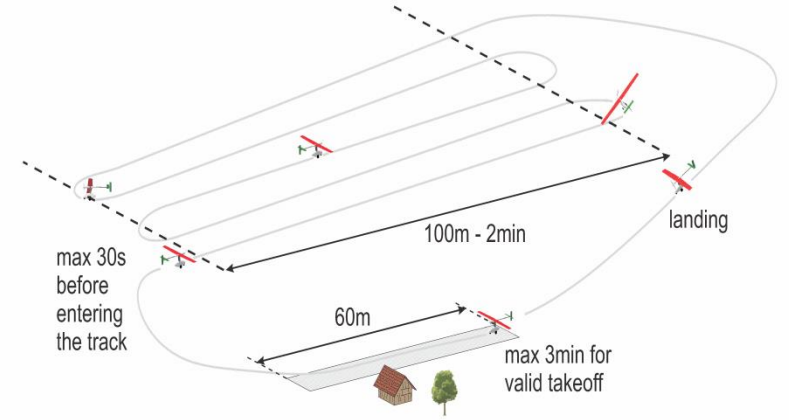

Fig. 1 Flight pattern
(Euroavia, 2015)

4. JUSTIFICATION

UPC Venturi was born to satisfy the necessity of multiple engineering students of applying theoretical concepts learnt at university, transforming them into a real project. Besides, this is an opportunity to acquire professional skills before leaving the academic ground and promoting entrepreneurship among students, hence being an added-value experience for companies. For this reason, our school dedicates resources every year, economic as well as work sites, to develop these projects in different grounds (aerospace, automotive, space…).

Since UPC Venturi was recently created in November 2014, one of the main difficulties of an organization with constant changes in its structure is to transfer knowledge and data from old members to the new ones after a project is finished. Since members leave as soon as they finish their studies and it is usual to struggle with time within the competition year due to the high work load, there is no time to close every phase documenting all the steps done. Therefore, it is crucial to set guidelines for members who join in so they can enroll faster, since their motivation is to learn and participate in useful tasks.

Regarding at technical part of the study, as a project manager I have been developing different aspects of the aircraft and acting as a merging person of the team, hence being as important to carry out communication tasks between departments as developing the project itself. From this broad point of view, it is also possible to find out which the main areas to improve are and where it is a substantial gain in competitiveness. This is the reason of starting the research on these areas and provide a first insight.

5. BACKGROUND

Aeromodelling has traditionally been a hobby where the aircraft can be hand-made with few materials, such as balsa, a cutter and glue. However, this kind of planes can only withstand low loads, leaving apart the case of acrobatic model aircraft. Nevertheless, when designing an Air Cargo Challenge plane, the score achieved depends on the payload carried. This means there are many aspects to have into account to avoid structural failure, provide enough stability and maneuverability and fulfill the requirements of the competition. In this context, higher technology and materials are required to achieve a competitive result.

Fig. 2 Pegasus II team, winner of the ACC 2007
Ensino Magazine Online, http://historico.ensino.eu/2007/out2007/universidade.html (accessed March 5, 2015)

Since this team was born to participate in the Air Cargo Challenge, it was a must to study the evolution of the aircrafts along previous editions, starting from 2007 at Lisbon. Previously, the competition took place in a national scope in Portugal. Since 2011, the ACC became an international event with teams from all over the world. Every two years, hundreds of engineering students meet at the ACC to share their knowledge rather than competing, as people are open to communicate with other teams than keeping their research hidden since the aim of the competition is to promote aerospace engineering and aeromodelling between students.

Through the past 8 years, there have been many changes on the design of these aircrafts, especially concerning materials and structural design. Regarding the aerodynamic study, it has been observed that similar airfoils and methodologies of study have been used. However, it is true that winners between 2009 and 2013 achieved a high lead thanks to an extended research on how to improve airfoil performance, in the case of AkaModell Stuttgart, a doctoral thesis aimed to design a high lift multi-element airfoil exclusively for this competition (Fig.3). In the case of the UBI team, winner of ACC 2011, a modification of the airfoil used by most of the participants, the Selig S1223, achieved similar results with an easier geometry to build wing structure.

Fig. 3 Aircraft from AkaModell Stuttgart, winner of the ACC 2013.
TeXtreme website, http://www.textreme.com/b2b/news-room/rg-and-textreme-helping-goliath-heron-to-win-the-air-cargo-challenge-2013 (accessed March 7, 2015).

Focusing on the structural and materials section, there has been a progressive substitution of wood parts by carbon fiber, which reduces significantly structural weight. In 2007, most of the teams used conventional structures with combination of balsa and plywood, meanwhile the winners used a D-box concept with a balsa main spar and the skin reinforced with glass and carbon fiber (Fig. 2). Obviously, the know-how of the Portuguese teams played a key role. Later, in 2009, a large number of teams included this concept to their planes, but the German team added an improvement using a composite of sandwich core made of Rohacell, carbon and glass fibers in all the skin surface.

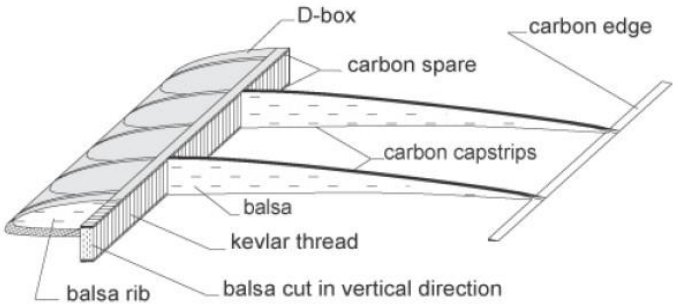

Fig. 4 D-box wing structural concept
http://file.espritmodel.com/documents/d_box_build/wing-structure.gif (accessed 2 May, 2015)

Since 2011, when the UBI team changed the structural concept to a single CFRP tube as a main spar instead of the D-box concept, most of the teams used it in 2013 because of its constructive advantages and high torsion stiffness. However, eventually, the German team won again in 2013 with the same concept that they used in 2009, showing that despite of having a complex structure, their results reaffirm this design (although it is difficult to judge the relevance of the structural part in their victory, since the aerodynamic research provides near 50% extra lift than conventional airfoils).

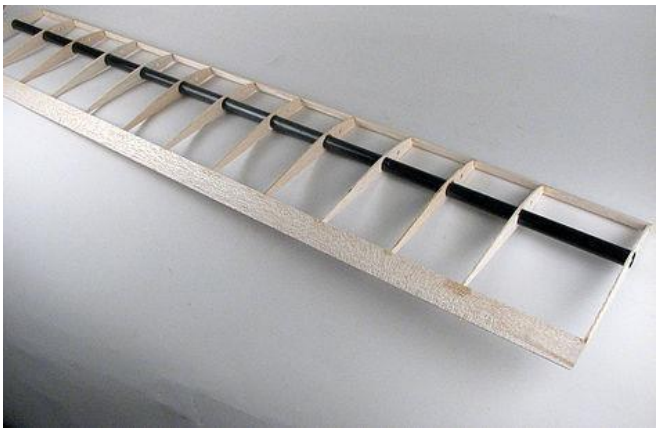

Fig. 5 CFRP tube wing structural concept
R&G website, http://www.r-g.de/wiki/Strangziehverfahren_(Pultrusion) (accessed 2 May, 2015)

6. HANDBOOK

6.1. Conceptual design

Starting to define the general concept of an aircraft is usually not an easy phase. As there are not many parameters fixed, there are multiple possibilities to combine and to study. In this chapter we will see which steps are needed to successfully complete this first approach to the design problem and the advantages and drawbacks of each layout will be shown.

The process followed is shown in the flow diagram below (Fig. 6). Between the possible conceptual layouts, Table 1 explains the different advantages and drawbacks from aircraft layout possibilities of every design.

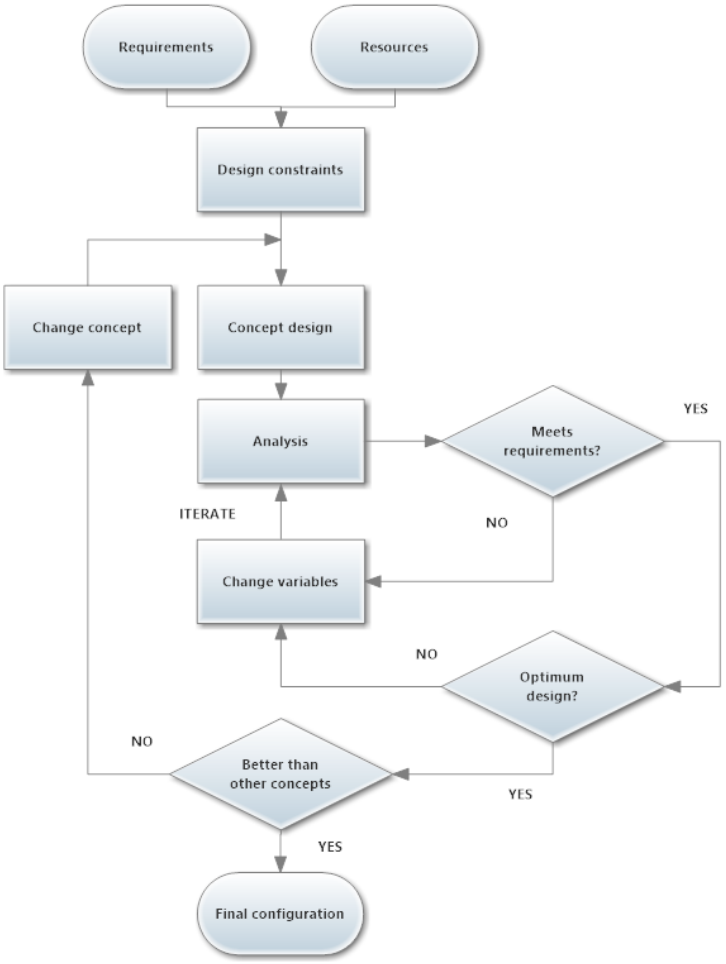

Fig. 6 Conceptual design flow diagram

Concept	Sketch	Advantages	Disadvantages
Low wing		• Short landing gear (low GC) • Easy access to payload	• Ground collision risk • Low lateral stability
Middle wing		• Lower aerodynamic interference	• Interaction cargo bay- wing beam
Upper wing		• Higher ground distance • Good lateral stability	• Less ground effect in T/O
Umbrella	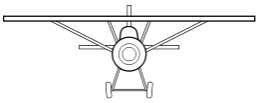	• Cleaner flow over the wing • High distance to ground • Good lateral stability	• Structural attachment to fuselage
Biplane	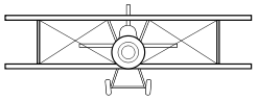	• Higher lift to the same projected area.	• Interference does not allow the production of the double amount of lift
Canard		• Stabilizer contributes positively to lift • Good longitudinal maneuverability	• Unstable near stall angles. • Residual fugoid modes
Tandem		• Higher lift keeping fixed span	• Rear wing in dirty flow. • Interference does not allow the production of the double amount of lift. • Stability problems • Super stall problem
Flying wing	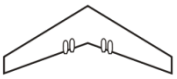	• Less drag	• Low Clmax • Unstable in high AoA configurations

Table 1. Aircraft configurations

Basically, what this diagram is stating is that since there is no close solution, first of all configurations that do not fit with the requirements and resources available must be discarded. Between the possibilities considered (or that there is no criteria to discard them before analysis), each one has to be optimized in function on predefined outputs in a preliminary design. The difficulty of this phase remains on the interaction between variables related to all fields of study. For instance, keeping a fixed wing surface, increasing span and reducing

chord leads to higher aerodynamic efficiency. On the other hand, larger span increases bending moment, requiring higher structural weight. Furthermore, unlike transport aircrafts, where there is a huge quantity of data and regressions to estimate coefficients at this early stage, there are few sources of information regarding analytical methods of model airplanes design. In this context, meeting mission requirements will limit the myriad of possibilities, but most of the times it will be useful to include extra restrictions or hypothesis to develop a preliminary design. Finally, once the solution is close to the optimal one, a final iteration including more parameters can be considered.

Regarding at the tail conceptual layout, the selection criteria is, as a general rule, determined by the position of the rest of the elements rather than being an optimization criteria. As a consequence, for example, in a turbojet aircraft with engine empennages attached to the fuselage, the tail cannot be placed behind the wake flow, acting as a design constraint. In the picture below (Fig. 7), there are different typical tail configurations. For our application, conventional tail (A-1, A-2) would be the most efficient in terms of structural weight, but T-tail (A-3) provides clean flow over the horizontal stabilizer, hence guaranteeing control during flight. Other groups such as B-2 can be considered when there is a large deflection of the boom tail. Group C is not widely used in this kind of aircraft because of the complexity of the control system, since both surfaces act as vertical and horizontal stabilizers.

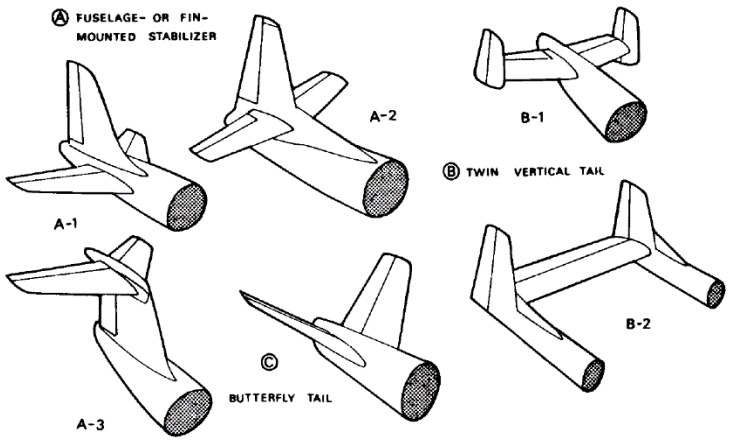

Fig. 7 Tail configurations
(Torenbeek, 1986)

6.1. Aerodynamics

When designing an aircraft, no matter its dimensions, it is important to define the scope of the aerodynamic study. Since both numerical capability and time are limited, there is a need of a compromise. In this chapter, the basic wing outputs will be exposed from a qualitative point of view.

6.1.1. Fundamentals of fluid mechanics

First of all, basics of theory behind flow over aerodynamic surfaces will be introduced. Before starting with the formulation of the problem, the variables and control of volume will be defined.

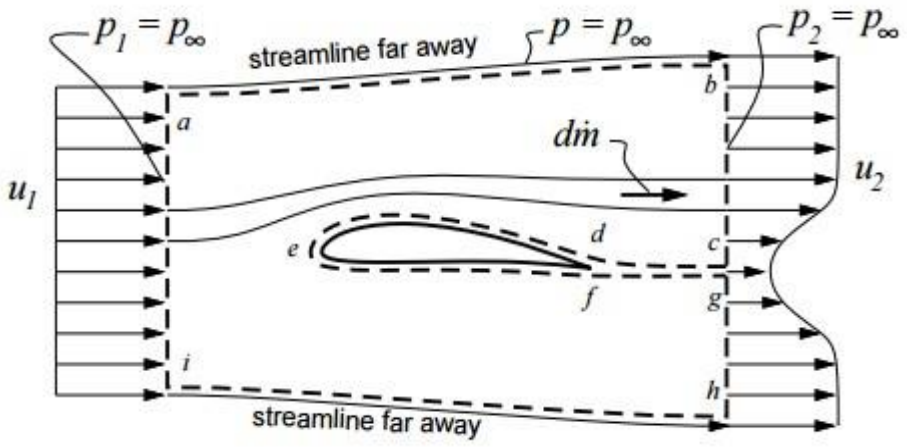

Fig. 8 Control volume to study effect of body in flow (Lozano, 2008)

Pressure at the intake (p_1) and outtake (p_2) far from the airfoil are the static pressure value, meanwhile speed distribution at the outtake (u_2) is affected due to the effect of the airfoil.

The surface integrals are now broken up into the individual pieces: the outer part *abhi*, the body surface *def*, and the "cut" surfaces *cd* and *fg*.

$$\oint ( )dA = \int_{abhi} ( )dA + \int_{def} ( )dA + \int_{cd} ( )dA + \int_{fg} ( )dA \qquad \textit{(Eq. 2)}$$

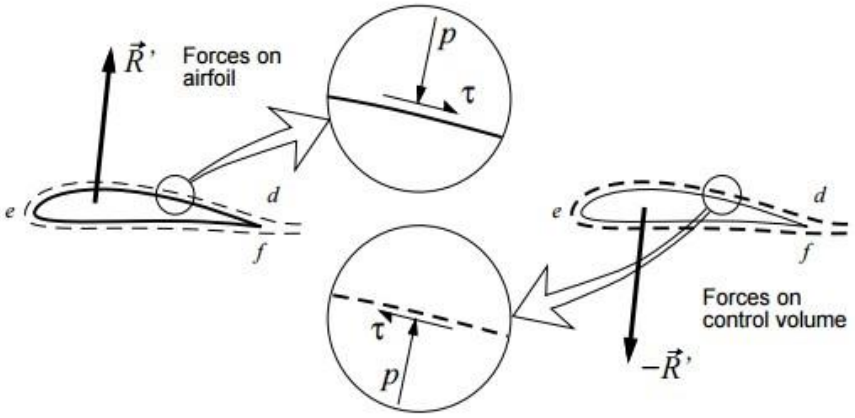

Fig. 9 Forces on the airfoil surface (Lozano, 2008)

Looking into detail what is happening along the airfoil there is a distribution of pressure and shear forces. The resultant force *R'* on the body is the integrated distribution of both on the surface. Because the body surface and volume surface have opposite normal directions *n*, this *R'* is precisely equal and opposite of all the def surface integrals for the control volume. An intuitive explanation is that the aerodynamic force exerted by the fluid on the body is exactly equal and opposite of the force which the body exerts on the fluid.

The next step is to identify the equations that govern the behavior of the fluid plus the boundary conditions.

- Continuity equation:

The principle of conservation of mass states that mass cannot be created nor destroyed. Therefore, if we consider a volume fixed in space, *V* , then the change of mass inside this volume can only take place if mass flows in or out through the boundary of this volume, *S*. Stated more precisely:

$$\frac{d}{dt}\int_V \rho dv = -\oint_S \rho u \cdot n ds \qquad \textit{(Eq. 3)}$$

After manipulating the expression, it can be obtained in differential form (Eq. 4):

$$\frac{\partial \rho}{\partial t} + \nabla \cdot (\rho u) = 0 \qquad \textit{(Eq. 4)}$$

- Momentum equations (3 components):

This equation is derived by assuming that Newton's 2nd law of motion is valid for any arbitrary volume cut out of the fluid. Thus, the rate of change of momentum of a fixed volume is the net momentum flux across the boundaries of the volume plus the net forces acting on the volume. Therefore:

$$\frac{d}{dt}\int_V \rho u dv = -\oint_S \rho u (u \cdot n) ds + \int_V \rho f dv + \oint_S n T ds \qquad \textit{(Eq. 5)}$$

Where T is the symmetric stress tensor which includes pressure and shear forces and f are body forces such as gravity.

$$T = (-p + \lambda \nabla \cdot \mathrm{u})\mathrm{I} + 2\mu \mathrm{D} \qquad \textit{(Eq. 6)}$$

In the same line that continuity equation, this expression can be written in differential form when applying Stoke's hypothesis for incompressible flow, which applies the expression $\lambda = -(\frac{2}{3})\mu^2$:

$$\rho\left(\frac{\partial u}{\partial t} + u \cdot \nabla u\right) = -\nabla p + \mu \nabla^2 u + \frac{1}{3}\mu \nabla(\nabla \cdot \mathrm{u}) + \rho \mathrm{g} \qquad \textit{(Eq. 7)}$$

- Energy equation:

$$\frac{d}{dt}\int_V \rho(e + \frac{1}{2}u^2) dv = -\oint_S \rho(e + \frac{1}{2}u^2) u \cdot n ds + \int_V u \cdot \rho f \, dv + \oint_S n \cdot (uT - q) ds \qquad \textit{(Eq. 8)}$$

Introducing the equation of momentum (Eq. 5) and manipulating the expression the simplified convective form is:

$$\rho \frac{De}{Dt} - T \cdot \nabla u + \nabla \cdot q = 0 \qquad \textit{(Eq. 9)}$$

Now that the formulation is clear, it is possible to come back to the airfoil to obtain the resultant R' through the momentum equation (Eq. 4):

$$\oint_{abhi} \rho(\vec{V} \cdot \hat{n})\vec{V} dA + \oint_{abhi} p\hat{n} dA = -\overrightarrow{R'} \qquad \textit{(Eq. 10)}$$

Despite having defined the problem (supposing that the boundary conditions are included), analytical solving of these coupled equations is not possible. Until computers appeared and could solve these equations numerically dividing the control volume into multiple finite volumes, aerodynamicists were forced to obtain results empirically or develope theories which included assumptions on these equations such as inviscid flow, linear methods, etc. (de Resende 2004).

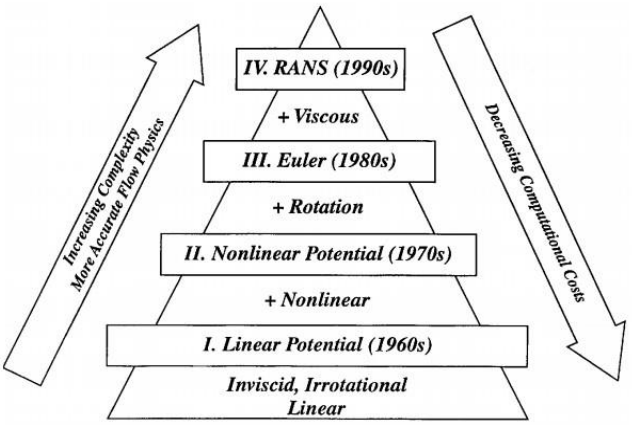

Fig. 10 CFD levels of analysis
Antony Jameson, Airplane Design with Aerodynamic Shape Optimization (Stanford, 2010)

6.1.2. Airfoil and wing parameters

Considering an airfoil such as the following one, the geometry is defined by the mean camber line, which is the curve of points halfway between the upper and lower surface measured perpendicularly to the camber, and thickness, which is also variable along the chord. The chord itself is defined as the line between the most forward and rearward points (leading edge and trailing edge, respectively).

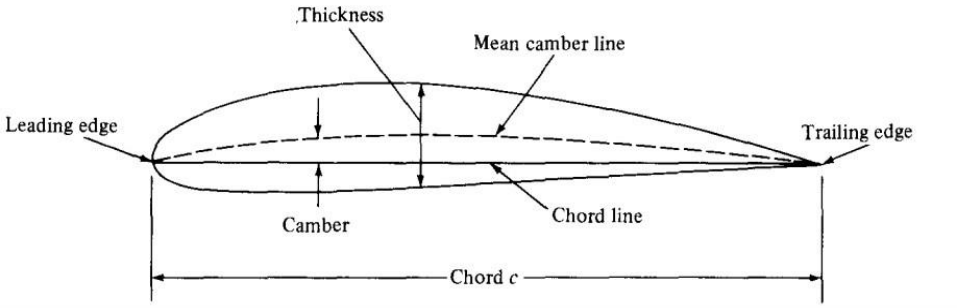

Fig. 11 Airfoil geometry (Anderson, 2005)

So as to study flow over the airfoil, the resultant force R' mentioned in the last section can be divided in two components, one is parallel to V_∞ which is relative wind speed measured to chord line direction, and the other one is perpendicular to V_∞. These forces are called lift and drag respectively. What is more, aerodynamic forces create a momentum which is defined at c/4.

From dimensional analysis, the following adimensional coefficients are used to compare airfoil parameters:

$$C_l = \frac{L}{\frac{1}{2}\rho {V_\infty}^2 S} \quad \textit{(Eq. 11)}$$

$$C_d = \frac{D}{\frac{1}{2}\rho {V_\infty}^2 S} \quad \textit{(Eq. 12)}$$

$$C_m = \frac{M}{\frac{1}{2}\rho {V_\infty}^2 Sc} \quad \textit{(Eq. 13)}$$

$$C_p = \frac{p - p_\infty}{\frac{1}{2}\rho {V_\infty}^2} \quad \textit{(Eq. 14)}$$

Once the velocity field has been solved, the distribution of pressure along the airfoil surfaces can be obtained, hence calculating the difference of pressure on the upper surface and the lower surface projected into the perpendicular direction to V_∞ provides the local lift distribution. This distribution of pressure is usually presented in an adimensional way, Cp. As it can be seen in the graph

bellow, most of the lift is generated close to the leading edge. The shape of this curves vary depending on the geometry, angle of attack and Reynolds number.

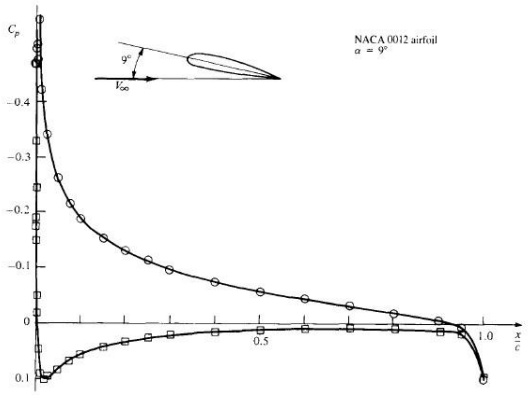

Fig. 12 Typical pressure distribution (Cp) over upper and lower surfaces (Anderson, 1991)

This C_{Lmax} point corresponds to the lowest speed at which the airplane in straight and level flight, called stall speed, V_s. Its equation is derived from L=W:

$$V_s = \sqrt{\frac{2W}{\rho S C_{L_{max}}}} \qquad \textit{(Eq. 15)}$$

In order to reduce V_s there are high-lift devices that allow to take-off in a shorter distance and landing at a lower distance, hence reducing the impact energy. The most common high-lift device are flaps, which increase camber and surface. Depending on their layout, they can also provide boundary layer control.

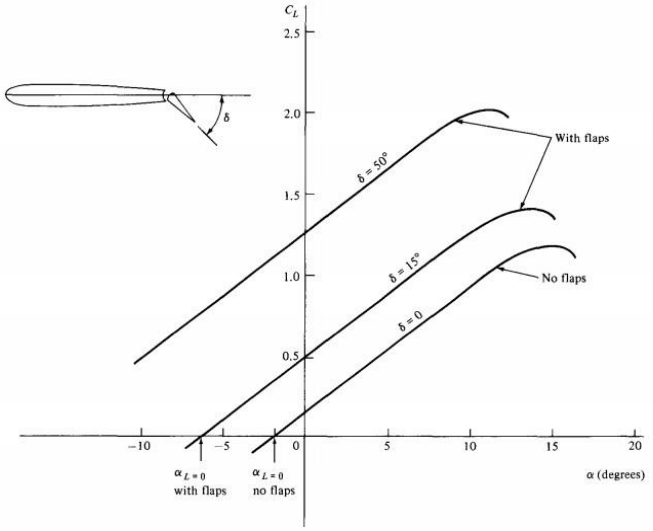

Fig. 13 Effect of flap on Cl at different deflections (Anderson, 2005)

This airflow study though, only considers 2D effects. When studying a wing, 3D effects appear. An intuitive explanation is that in finite wings the upper surface has lower pressure than the lower surface, hence there is a difference of pressure in the wing tip, creating a flow from the lower to upper surface. This flow establishes a circulatory motion which trails downstream of the wing called vortex. These vortex induce a downwash component of speed in every section of the wing, *w*. As it can be seen in Fig. 12, this component reduces local effective angle of every airfoil.

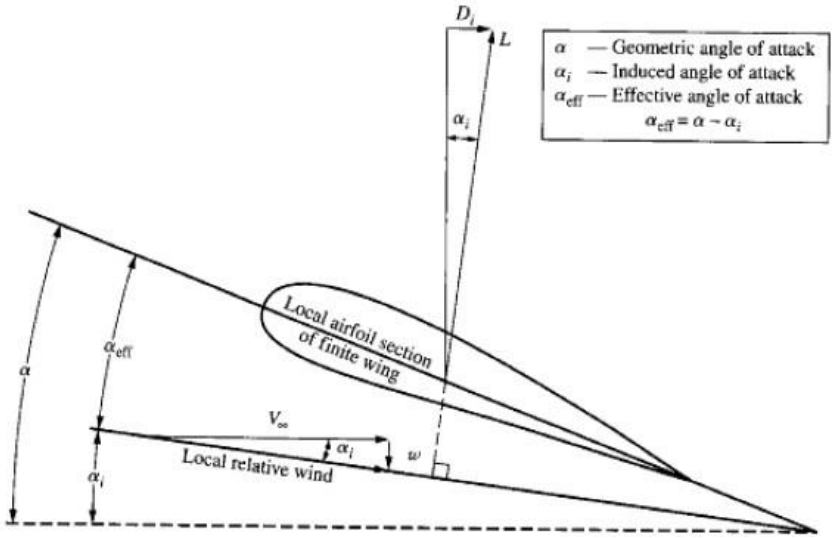

Fig. 14 Effective alpha due to induced angle following Prandtl wing theory (Anderson, 1991)

The contribution of this induced angle increases drag and reduces lift as follows:

$$C_d = C_{d,profile} + \frac{{C_L}^2}{\pi e\, AR} \qquad \textit{(Eq. 16)}$$

Where e is the span efficiency factor and AR (aspect ratio)= $\frac{b^2}{S}$. For elliptical planform, e=1, the rest have a lower value, hence being less efficient. From this analysis, one can appreciate that when aspect ratio tends to infinity 3D effects are reduced, hence Cd is closer to Cd,profile. However, in real aircrafts this value does not use to be larger than 10-15 due to structural loads, since higher span leads to higher bending moment (section 6.5.1.).

When designing the wing geometry, other aspects such as aerodynamic torsion or dihedral can be considered, but they are not always functional since the manufacturing process is more complex.

6.1.3. XFLR5

XFLR5 is a free source software developed by M. Drela which is based on a coupled panel method/boundary layer code. The method is a 3D analysis whose results are obtained from an inviscid linear-vorticity panel method, but data input includes a 2D boundary layer model to capture separation bubbles and predict drag coming from viscous layers. Despite of including only inviscid 3D drag effects, XFLR provides reliable data when analyzing low Reynolds flows (<500.000).

This tool has been used during the project as it has been designed especially for low Reynolds aircrafts. Despite of not providing high accuracy results (experimental results couple with XFLR5 results but the margin of error depends on the analysis conditions), this software allows a good preliminary design criteria. For further information, attachment A.1 contains a tutorial with some recommendations and considerations when using the software.

6.2. Propulsion and performance

Propulsive systems allow not only to accelerate the aircraft, but to balance out aerodynamic drag and friction along the runway. This means that as a first idea, selecting a higher power engine provides larger possibilities to improve maneuverability provided that the rest of the airplane is capable to withstand the forces generated. This is a general characteristic, not only for the ACC. As we will see, propulsion is closely related to the next section: performance, stability and control.

The predicted thrust is assumed to be governed by the following analytic expression derived from blade element theory:

$$T = k^2 \cdot \pi^2 \cdot c \cdot \frac{1}{2} \cdot \rho \cdot n^2 \cdot D^3 \cdot \left(C_L - \frac{2J}{k}\right) \cdot \sqrt{1 + (\frac{J}{k \cdot \pi})^2} \cdot [1 - \frac{J}{k \cdot \pi} \cdot \tan(\gamma)] \quad \textit{(Eq. 17)}$$

However, this equation contains lots of terms which are unknown depending on the geometry of the blade. Since both, motor and propeller, were fixed in this ACC edition, there is no possibility to study alternatives to the configuration of AXI Gold 2826/10 plus an APC 13x7" Sport propeller. This requirement allows an easier study of the propulsive system. Looking for extra sources of information we found an experimental study from the Illinois Institute of Technology which functionally matched our motor-propeller composition (AXI Gold 2826/10 plus an APC 13x6.5") and it has been source of data since it would more accurate than an analytical result since static thrust prediction overestimates the real thrust as seen in Fig. 15. For a more accurate thrust modelling, an experimental study should be done but was not considered in the scope of this project due to the lack of resources, since the wing tunnel of our university did not meet the dimensions.

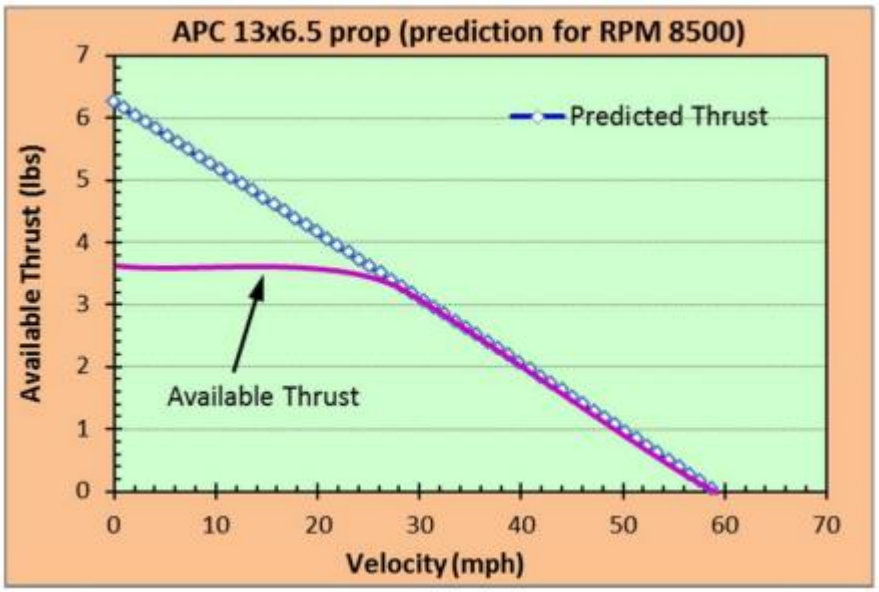

Fig. 15 Thrust vs speed experimental study
Dr. Murat Vural, http://mypages.iit.edu/~vural/RC%20Airplane%20Design.pdf (accessed 15 March, 2015)

From this point, coupling the thrust available with flight mechanics, it is possible to obtain the performance equations of the aircraft. From 2nd Newton's

law, the forces applied to the body determine all the accelerations. These equations will be implemented in the Matlab codes later.

General dynamic equations, using wind axis (x_w, y_w, z_w):

$$x_w:\ T \cdot Cos(\alpha) \cdot Cos(\varepsilon) \cdot Cos(\nu) - D - W \cdot Sin(\gamma) - m \cdot V_\infty = 0 \qquad \textit{(Eq. 18)}$$

$$y_w: -T \cdot Sin(\varepsilon) - L + W \cdot Cos(\gamma) \cdot Cos(\mu) + m \cdot V_\infty \cdot \left(\dot{\gamma} \cdot Cos(\mu) + \chi \cdot Cos(\gamma) \cdot Sin(\mu)\right) = 0 \qquad \textit{(Eq. 19)}$$

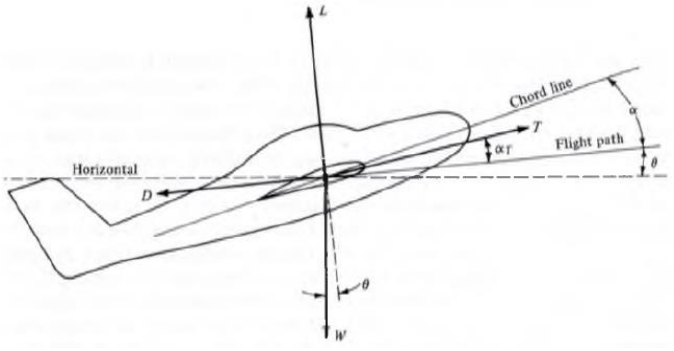

Fig. 16 Forces diagram on an aircraft (Andersson, 1991)

6.2.1. Simmetric flight

From these equations, assuming wings leveled ($\mu = 0$), plane maintaining altitude ($\gamma = \dot{\gamma} = 0$), no thrust vectoring or incidence ($\varepsilon = \nu = 0$) and no yaw ($\chi = 0$) the equations are reduced to:

$$x_w:\ T \cdot Cos(\alpha) - D = m \cdot \dot{V_\infty} \qquad \textit{(Eq. 20)}$$

$$z_w: -L + W = 0 \ \rightarrow Load\ factor\ n = \frac{L}{W} = 1 \qquad \textit{(Eq. 21)}$$

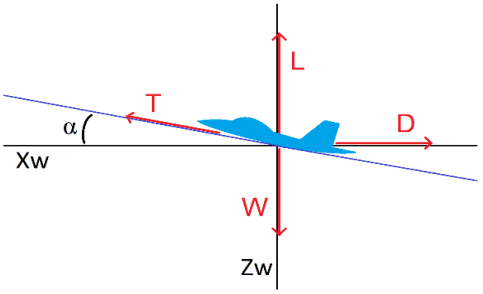

Fig. 17 Simmetric flight forces diagram

Kinematic equations, using horizon axis (x_h, y_h, z_h):

$$x_h: \ \dot{x}_h = V_\infty \cdot Cos(\gamma) = V_h \qquad \textit{(Eq. 22)}$$

$$z_h: \dot{z}_h = -V_\infty \cdot Sin(\gamma) = 0 \qquad \textit{(Eq. 23)}$$

Coupling the power available (Eq. 22) and the required power from polar curves (Eq. 23), the maximum speed is obtained when the aircraft reaches the intersection of both. That means the maximum thrust available is equal to drag in levelled flight (obviously the speed could be increased but losing potential energy from altitude).

$$P_a = T(V_\infty) \cdot V_\infty \qquad \textit{(Eq. 24)}$$

$$P_n = D(V_\infty) \cdot V_\infty = \frac{1}{2} \cdot \rho \cdot V_\infty^2 \cdot S \cdot C_D \cdot V_\infty \qquad \textit{(Eq. 25)}$$

6.2.2. Coordinated turn in a horizontal plane

Assuming wings are not level ($\mu \neq 0$) but no there's no lateral drift ($\beta = 0$) the following equations provide information about a turn without losing potential energy ($\dot{z}_h = 0$).

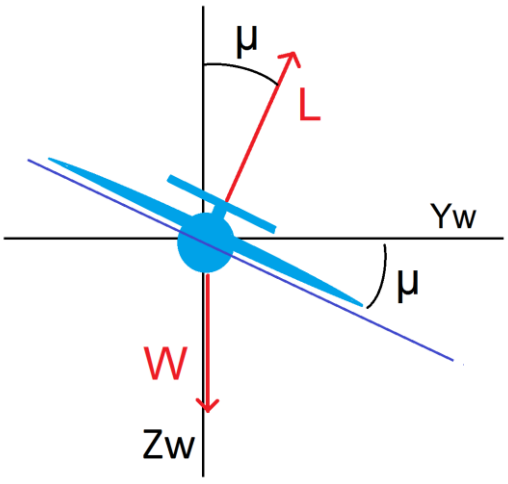

Fig. 18 Coordinated turn

General dynamic equations, using horizon axis (x_h, y_h, z_h):

$$x_h: \ T \cdot Cos(\alpha) - D = m \cdot a_t \qquad \textit{(Eq. 26)}$$

$$y_h: L \cdot Sin(\mu) = m \cdot a_c \qquad \textit{(Eq. 27)}$$

$$z_h: W = L \cdot Cos(\mu) \qquad \textit{(Eq. 28)}$$

Where $a_t = \Delta U_\infty / \Delta t$ is tangential acceleration, $a_c = \frac{U_\infty^2}{R} = R \cdot \omega^2$ is centripetal acceleration, $\omega = \frac{\Delta\theta}{\Delta t}$ is angular speed and from eq. 29, it is deduced that $L \neq W$ and $n = \frac{1}{Cos(\mu)} > 1$. Coupling these equations these expressions for the radius and angular speed are obtained:

$$R = \frac{U_\infty^2 \cdot m}{L \cdot Sin(\mu)} \qquad \textit{(Eq. 29)}$$

$$\omega = \sqrt{\frac{L \cdot Sin(\mu)}{R \cdot m}} \qquad \textit{(Eq. 30)}$$

6.2.3. Climbing angle

From the equations of levelled flight without the condition of maintaining altitude ($\gamma \neq 0$), it is possible to calculate the maximum angle of climbing from the difference between power available and power required.

$$\sin\gamma = \frac{P_a - P_n}{m \cdot g \cdot V_\infty} \qquad \textit{(Eq. 31)}$$

6.2.4. Take-off

In the case of the take-off analysis, UPC Venturi has developed another Matlab code which divides the run in multiple sections to iterate a numerical resolution governed by this integral-differential equation derived from Newton's

second law. After working with this equation it is possible to obtain the MTOW for every layout.

$$s = \frac{1}{m}\int_0^{k^2\sqrt{\frac{2mg}{\rho S C_{Lmax}}}} \frac{v \cdot dv}{T(V_\infty) - \frac{1}{2}\rho v^2 S C_D(V_\infty) - \mu\left(mg - \frac{1}{2}\rho {V_\infty}^2 S C_L(V_\infty)\right)} \quad \textit{(Eq. 32)}$$

Where k (safety factor from stall speed)= 1,05, s (runway length)= 60 m, g=9,81m/s^2, μ=0,8 (rubber on concrete), ρ=1,202 kg/m^3 (Stuttgart density). The rest of parameters are imported from XFLR5: S, C_{Lmax}, $C_L(V_\infty)$, $C_D(V_\infty)$.

6.3. Structural design

The main objective of the structural design is to prevent structures from permanent deformation or failure when reaching ultimate load conditions keeping the lowest weight possible. Furthermore, it has a vital importance to design paying attention to the manufacturing processes involved. In this section the basics of the theory behind structures dimensioning will be presented, focusing on the wing structure.

6.3.1. Elastic beam theory

To understand the concepts that will be presented later, a brief explanation of the fundamentals of structural mechanics will be introduced.

The elastic beam theory is derived from several principles. The internal equilibrium equations ($\sum F = 0$ and $\sum M = 0$ for the three axis) states that when a body is applied with external loads, internal forces appear to keep this equilibrium.

In a beam differential, suppose an external force vector per length unit *q(x)* and a moment per length unit *m(x)* as shown in Fig. 24.

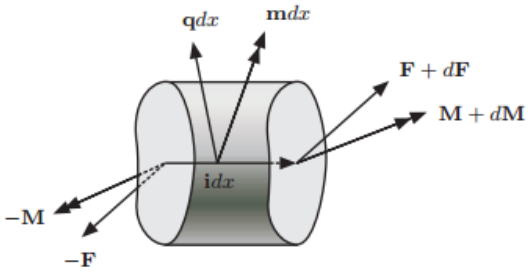

Fig. 19 Internal equilibrium in elastic beam
Andersen, L., Nielsen, S.R.K.. Elastic Beams in Three Dimensions. http://homes.civil.aau.dk/jc/FemteSemester/Beams3D.pdf [Accessed May 5, 2015].

If these reactions are decomposed in three axes as shown in Fig. 20 and these expressions are introduced into equilibrium equations, the result are Eqs. 33 and 34.

$$\frac{dN}{dx} + q_x = 0 \; ; \frac{dQ_y}{dx} + q_y = 0 \; ; \frac{dQ_z}{dx} + q_z = 0 \qquad \textit{(Eqs. 33)}$$

$$\frac{dM_x}{dx} + m_x = 0 \; ; \frac{dM_y}{dx} - Q_z + m_y = 0 \; ; \frac{dM_z}{dx} + Q_y + m_z = 0 \qquad \textit{(Eqs. 34)}$$

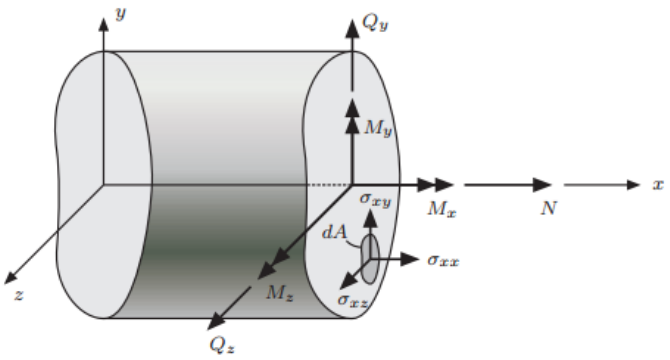

Fig. 20 Stresses in elastic beam
Andersen, L., Nielsen, S.R.K.. Elastic Beams in Three Dimensions. http://homes.civil.aau.dk/jc/FemteSemester/Beams3D.pdf [Accessed May 5, 2015].

Next, these reactions can be defined as an integration of stresses along the section $(\sigma_{xx}, \sigma_{xy}, \sigma_{xz})$. From this point, developing the kinematics and deformation beam equations, it is possible to relate normal stresses to geometrical and material properties of the section (Eq. 35). Note that this

formulation is valid for generic axes located in the centroid of the section in isotropic beam.

$$\sigma_{xx}(y,z) = \frac{N}{A} - \frac{M_y I_{yz} + M_z I_y}{I_y I_z - {I_{yz}}^2} \cdot y + \frac{M_y I_z + M_z I_{yz}}{I_y I_z - {I_{yz}}^2} \cdot z \qquad \textit{(Eq. 35)}$$

In order to calculate these geometrical parameters of the section, the area, centroid position and the inertia in both axes are required. These expressions are calculated as a summation of individual parts of the structure (since it will be more functional than integrating generally).

$$A = \sum_{i=1}^{N} A_i \qquad \textit{(Eq. 36)}$$

$$Y_C = \frac{\sum_{i=1}^{N} A_i\, y_i}{A};\ Z_C = \frac{\sum_{i=1}^{N} A_i\, z_i}{A} \qquad \textit{(Eq. 37)}$$

$$I_{yy} = \sum_{i=1}^{N} A_i\, {x_i}^2;\ I_{zz} = \sum_{i=1}^{N} A_i\, {z_i}^2;\ I_{yz} = \sum_{i=1}^{N} A_i\, y_i z_i \qquad \textit{(Eq. 38)}$$

From the shear stresses $(\sigma_{xy}, \sigma_{xz})$ derived from the bending moment or an external torque applied, there is a distribution of forces in the section walls that tend to slide or rotate sections between each other. The equations governing these phenomena are derived from the Collignon theorem, which states that in a beam section with a differential length, the difference between normal stresses requires a shear stress to accomplish the equilibrium of internal forces. This shear stress in an imaginary cut of the section follows (Eq. 39 when not operating with principal axes, as a medium value.

$$(\tau_{nx})_{med} = \frac{Q_y I_{yy} - Q_z I_{yz}}{I_y I_z - {I_{yz}}^2} \cdot \frac{{m^*}_z}{L_{ab}} + \frac{Q_z I_{zz} - Q_y I_{yz}}{I_y I_z - {I_{yz}}^2} \cdot \frac{{m^*}_y}{L_{ab}} \qquad \textit{(Eq. 39)}$$

Where ${m^*}_z = \iint_{S^*} y ds$ and ${m^*}_y = \iint_{S^*} z ds$, being S^* the resulting surface of the cut. L_{ab} corresponds to the length of the cut.

When working with thin walls, the importance of these tangential stresses in front of normal ones gets more importance, simplifying the calculation. Derived from the equilibrium in a panel as a product of a cut, it is possible to obtain the

distribution of shear flow, which is defined as $q = \tau \cdot t$, being t the thickness of the wall. The procedure is to cut the closed profile as it follows:

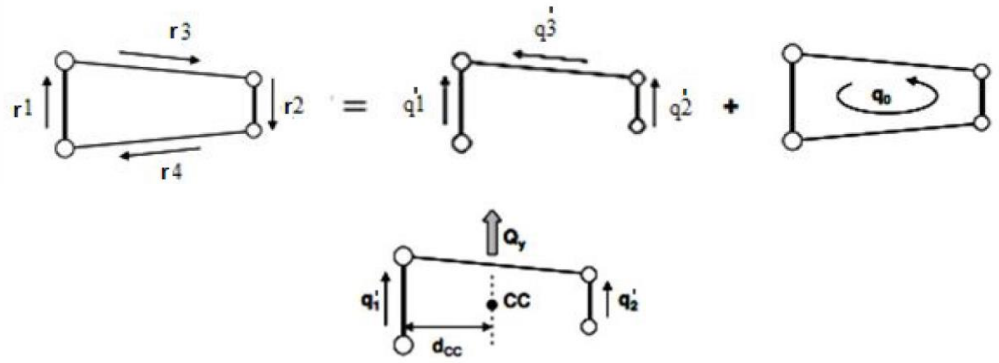

Fig. 21 Distribution of shear flow in wing box

In this case, principal axes can generally be used since there are symmetry axes (note that now *x* axis is in chord direction, *y* in span direction and *z* is vertical in the section plane). The formulation for the open profile of the shear flow follows equation (Eq. 40. The difference between shear flow is produced in every cordon.

$$q_i = q_o - \frac{Q_y}{I_{zz}} \sum_{j=1}^{i} y_j S_j - \frac{Q_z}{I_{yy}} \sum_{j=1}^{i} z_j S_j \qquad \textit{(Eq. 40)}$$

In attachment A.4 there is a detailed explanation of how to use this method in order to find the distribution of shear stresses analytically.

6.3.2. Wing loads

During the design of a wing, stresses produced by the effect of external loads such as aerodynamic forces, payload of thrust are considered in order to choose the right materials and geometry.

In order to complete a full analysis, the distribution of pressure over all wing surfaces should be included in the methodology as shown in. Nevertheless, this method is not functional unless we are working with a coupled CFD-structural analysis through finite volumes method as it will be shown in 8.2. FSI study.

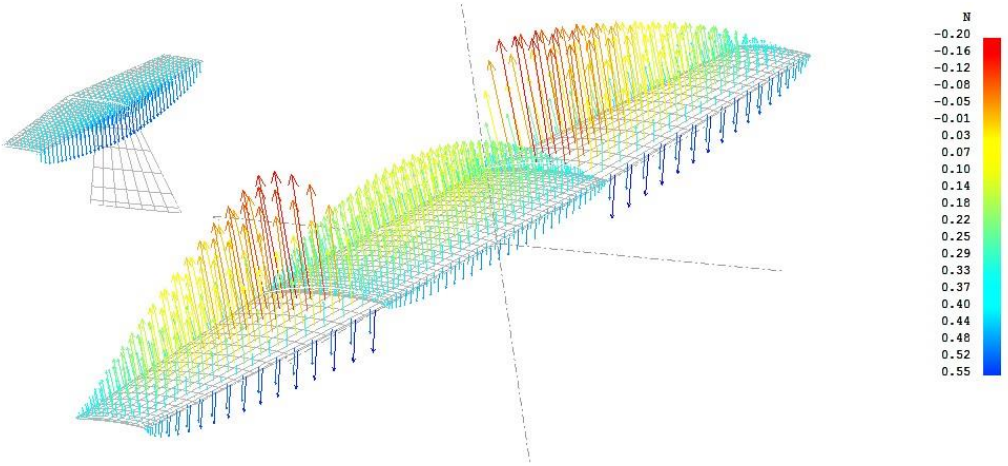

Fig. 22 Distribution of aerodynamic forces in XFLR5

Assuming several hypothesis obtained from the bibliography (Bruhn & Bollard, 1973), it is possible to get reasonable results with analytical results. Applying the concepts mentioned before about beam theory to a wing, it is possible to calculate the distribution of the internal reactions. Drag forces could be included in this first analysis, but as a first approach only lift will be considered (as an order of magnitude, ratio between them is 1:10).

$$Q_z(y) = -\int_{b/2}^{y} l(y)\, dy \sim -\sum l_i \Delta y \qquad \textit{(Eq. 41)}$$

$$M_x(y) = -\int_{b/2}^{y} l(y) y\, dy \sim -\sum l_i y_i \Delta y \qquad \textit{(Eq. 42)}$$

6.3.3. Wing design

In order to withstand these reactions, the wing structure has typically been divided in different components, each one focused on different stresses. Generally, wings are made of these parts:

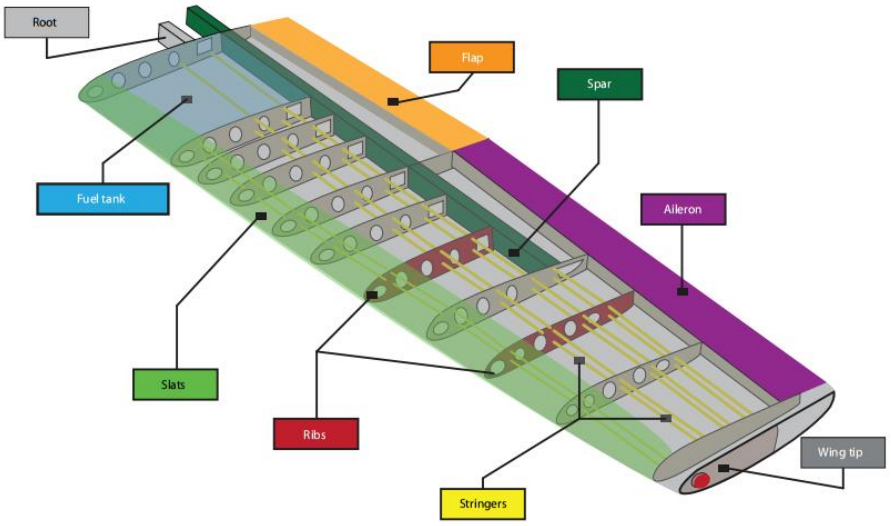

Fig. 23 Wings components
NASA, Parts of an aircraft: Wing design. http://www.aeronautics.nasa.gov/pdf/wing_design_k-12.pdf [Accessed May 2, 2015].

- Skin: It is the aerodynamic shape of the wing. As it has the higher inertia fibers, it should stand a great part of the longitudinal stresses (σ_{xx}) due to Mz distribution. Besides, as part of the closing walls of the profile, stands shear stresses.
- Ribs: Transversal components that provide the shape of the airfoil and prevent the skin from buckling (instability due to non-linear effects).
- Spars: As main elements of the wings (one or more) they transfer the loads from the ribs and stand shear stresses, as well as part of the longitudinal stresses.
- Stringers: Beams in the longitudinal axis providing stiffness to the skin. Limiting the free space between ribs and stringers, wing panels are smaller, hence buckling is avoided since it depends on this free space (among other factors).

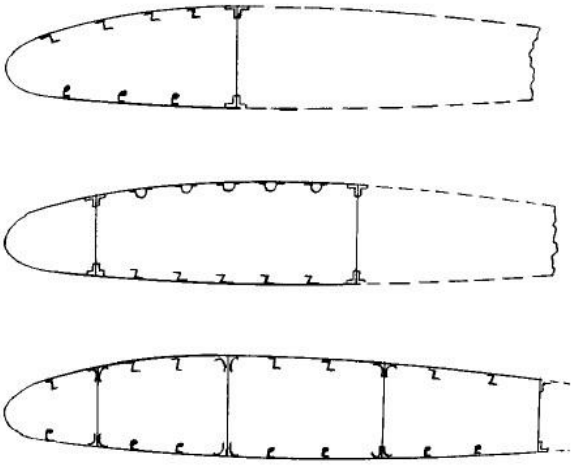

Fig. 24 Wing structure examples: D-box, torsion boxes (Bruhn & Bollard, 1973)

6.4. Materials

One of the main problems when designing a component is that new members who have little or none experience with model airplanes is that it is difficult to choose which materials to use and their dimensions. Obviously, an analytical dimensioning or finite element calculation provides a better criteria, but the intuitive idea after touching the different materials and checking their stiffness allows to have an idea of the materials and dimensions required.

In order to make the right choice of materials, it must be had into account the kind of stresses that they will be supporting and the properties of the material itself. First of all, we must classify them in isotropic ones, whose properties do not depend on any direction (steel, aluminum...), and anisotropic materials, which have different properties for every direction (wood, carbon fiber).

6.4.1. Balsa

Balsa wood stands as a very light material, ideal for aeromodell applications. Nevertheless, it can be shattered when applying forces in the transversal direction due to the orthotropic behavior of the fibers. Balsa ribs will be typically used in parts with low structural load, acting as form ribs to ensure the

aerodynamic airfoil shape and limiting the buckling of the rest of the elements. In the case of ribs connected to other components of the aircraft, balsa is not recommended if there is a transmission of stresses.

Typical thickness range is between 1 and 3 mm. In the case of using this material to recreate the shape of the leading edge (for example in a D-box structure), it may be reasonable choice since wetting the balsa sheets the material becomes very flexible and adapts to curved forms such a tube. This process should be repeated several times in order not to brake the sheet. For the case of the leading edge and tail ribs 1mm thickness is recommended, whereas for wing ribs 2mm thickness allows a higher surface of contact to iron out the plastic cover.

6.4.2. Plywood

Plywood composites are made of a group of wood sheets laid in different directions in order to avoid the anisotropic behavior of wood. In this case, plywood has a more general application since it can be used in all types of structures where balsa would not be used. The drawbacks of using this material also have to be taken into account since density is higher and laser cutting requires more time, hence increasing the budget of the project.

Recommended value for plywood sheets thickness is 2 mm for ribs or structures withstanding high loads (for instance a landing gear). Lower value of thickness leads to deformation of the rib before loading.

6.4.3. Carbon/glass fiber

During the last decades, the application of carbon fiber in aerospace field has constantly increased. Due to its high strength to weight ratio, it provides lighter structures than typical metal-based alloys. Moreover, carbon fiber presents a high elastic module, leading to stiff structures. The main drawback remains on the manufacturing technology, which requires high expertise and the design is often restricted by the manufacturing process. Furthermore, these composites present low damage tolerance, so they are not used in structures such as leading edges

where there can be impacts because of birds. In our application, it is important to pay attention to structural parts where this kind of dynamic stresses appear, such as the landing gear. In the case of glass fiber composites, same philosophy is applied, although comparing to carbon fiber, it provides a lower strength to weight ratio at a lower price.

Carbon fiber-based composites are classified by the way the manufacturing process and their geometrical properties. The former corresponds to composites called preimpregnated, which is bought already laminated, or buying the carbon fiber cloth plus the matrix (usually epoxy or polyester resin) and laminating over the surface intended to be reinforced. The other classification corresponds to carbon fiber preimpregnated or cloth where properties are unidirectional (all the fibers are aligned in the same direction) or orthotropic direction, where fibres are distributed in 0-90º or 45º. In the case of unidirectional composites it is recommended to encircle the surface with Kevlar strings to prevent the material from delamination due to transversal stresses. For cloth material, the lowest surface density is recommended, with values between 70 and 100 g/m^2.

Preimpregnated composite has an optimal finishing compared to handmade laminated sheets, with a proper manufacturing process which includes curing at 70-80ºC of the composite. Nevertheless, these sheets cannot be used when defining a complex surface. In the case of designing a wing skin for instance, the only option would be to design a mold and cure the cloth with the matrix at the workplace. Curing the composite at the temperature mentioned instead of ambient temperature increases the tensile strength of the material.

Regarding at the self-prepared composites from the fiber clothes, there are different techniques to create carbon fiber composites. Depending on the type of geometry one or other are recommended. In the case of shapes with low curvature, using pressure molds as male and female can work out and place the reinforcement containing the epoxy resin inside straight forward, only needing a release agent for the mold.

Another technique is to use vacuum bagging. This is a good practice especially when there are complex shapes. It consists of distributing the pressure

with a vacuum pump instead of a pressure mold (Fig. 25). Aknowledgements to Compolab for providing us with the materials required to this process.

Fig. 25 Self-made carbon fiber part with vacuum bagging

Due to the lack of resources, it has been impossible mechanize molds for complex parts and wing structures, since they require CNC technology which is unaffordable. As it will be discused later, achieving an sponsorship for these molds or building them ourselves could be a remarkable improvement.

6.4.4. Foams

Foams have become one of the most popular materials for conventional RC airplanes due to its low cost and density. Moreover, they usually present isotropic properties, simplifying the structural design. In our application, foams themselves cannot provide enough stiffness of the structure, so they will be used as part of composites, typically in sandwich structures.

There are two main applications of foams, one is to prevent buckling from other components and the other is to provide inertia to other high modulus materials acting as a core in beams. Some examples of useful foams for our application are Depron and Rohacell, which can be used in ribs as well.

6.4.5. Covers

Covers are thermoretractable materials which are used as skin in traditional aeromodell structures. Since they are ironed to get attached to ribs, due to its thermoretractable properties it acquires a tensioned state that provides torsion stiffness.

6.5. CAD/CAM

Creating a 3D plane in Catia or Solid Works is necessary to cut the ribs or plane parts whose geometry requires high accuracy. This process demands the collaboration of external companies which use laser cutting machines with CNC. An extensive guide on how to create 3D geometries from coordinates is included in attachments (A.2). The generation of the wing structure used in the ACC 2015 and the torsion box alternative presented in section 8.1 has exclusively been part of this study, while other components have been created by other team members.

The 3-view and isometric drawings of the aircraft are included in the Drawings document to provide a general idea of the layout to the reader, rather than fulfilling rigorous standards since they were made for the ACC final report.

7. AIRCRAFT FOR THE AIR CARGO CHALLENGE

In this section a summary of the decisions, justification and results of the design and geometry chosen will be presented.

7.1. Preliminary design

Regarding at the aircraft layout and conceptual design, after developing a Matlab code which could predict the score, several configurations with simplified concepts were tested to identify tendencies on which parameters were decisive. This iteration process following *Fig. 6 Conceptual design flow diagram* leaded to the final layout. Between the possibilities considered, the rejected some designs due to the lack of accuracy analysis in the case of canard and biplane concepts, such as interaction between wings in XFLR5, and flying wing because of not being competitive due to $C_{L_{max}}$. The chosen solution was a conventional aircraft with T-tail.

This Matlab code, included in attachment A.3 (acknowledgements to Alejandro Ibáñez for implementing part of the code), was developed to compare different aircraft wing configurations in function of the score that the code predicts that each setup will achieve. This script used both from theoretical aerodynamic data generated with XFLR5 software and propulsion experimental data –presented later on the corresponding chapters– and used it to predict how many laps the airplane would achieve with different payloads. On the first iterations, a standard wing was designated to compare the performance of several airfoil shapes and later, many wing layouts were put to test in different variations of span, chord and payload using the most promising airfoils found in the previous analysis.

Every member of the team presented an excel worksheet presenting his assigned airfoil in order to establish the general direction in which the airplanes performed better. The script helped to identify that larger wing surfaces allow for

greater payloads which in turn lead to the design of the longest wing possible with a rather large chord, hence increasing payload instead of speed.

Next step was to design the tail stabs and adjust the distance from the horizontal tail plane –HTP– to the wing so that the whole airplane can rest inside a 2,5 x 2,5m square without parts protruding meeting the requirements of the regulations. At the same time the static and dynamic stability of the aircraft had to be considered when manipulating the distance to wing, shape, surface and incidence of the HTP. The tail is placed at the most rearward position since it is the option which creates the same negative lift with a lower drag due to a reduced angle of attack.

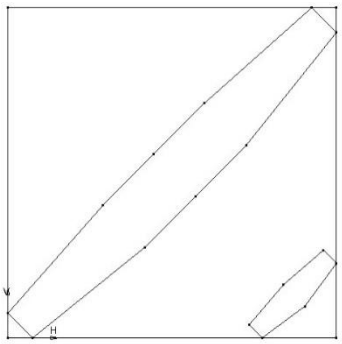

Fig. 26 Sketch checking 2,5x2,5 m2 box fitting

After that, a different Matlab script was used to solve the take-off equation (Eq. 32) and more analysis with XFLR5 were carried out introducing simple flaps in order to calculate the maximum payload possible to take-off within the 60m of runway available. After some iterations calculating maximum payloads and their score, the airfoil was selected.

7.2. Aerodynamic results

The results of this section correspond to the conclusions of all the team members' work. The software used has been XFLR5.

7.2.1. Airfoil analysis

As a direct result from the Matlab predictions we have chosen the airfoil SG6042 shown below, which was obtained from UIUC Airfoil database.

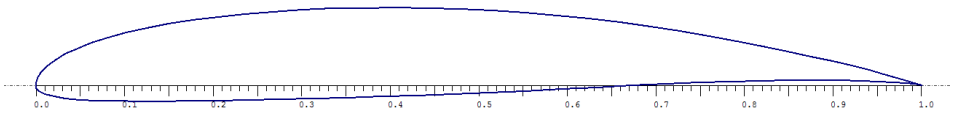

Fig. 27 SG6042 airfoil

Max thickness 10% at 33.5% chord.
Max camber 3.3% at 51.5% chord

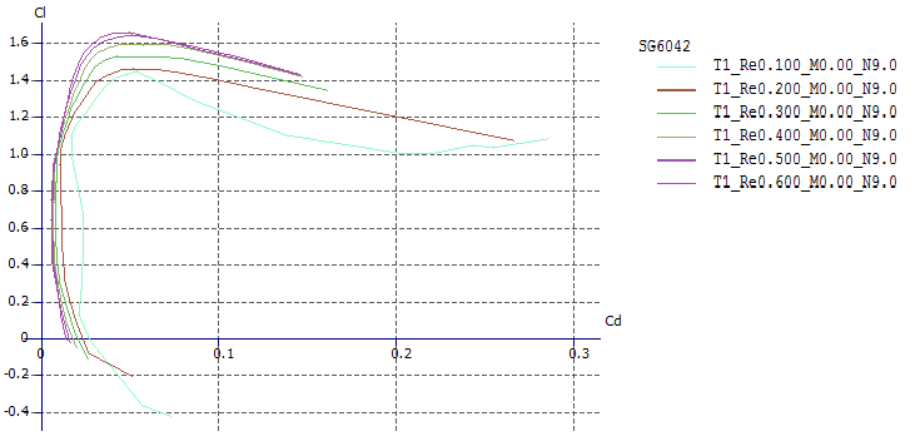

Fig. 28 Cl vs Cd polar graph

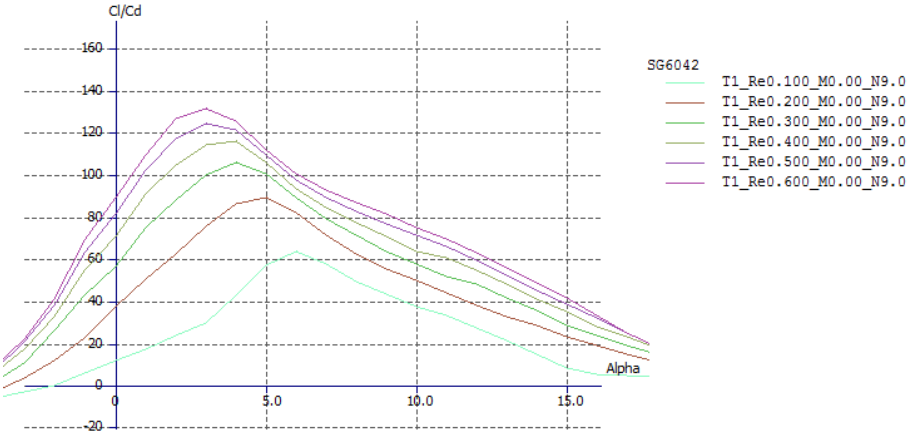

Fig. 29 Cl/Cd (1/Glide angle) vs alpha

In addition of providing a high score, the SG6042 features very interesting geometric parameters for structural analysis (maximum thickness is close to the *x* coordinate where the CoG should be located, which usually is around 30% of the wing chord, so that the inertia for the main wing spar could be optimized). Moreover, the trailing edge is not very sharp (easier to build) and it offers a relatively flat underside surface (good for the Oracover ironing process).

7.2.2. Wing analysis

	y (mm)	chord (mm)	offset (mm)	dihedral	twist(°)	foil	X-panels	X-dist	Y-panels	Y-dist
1	0,000	450,000	0,000	0,0	0,00	SG6042	13	Cosine	19	-Sine
2	545,000	450,000	0,000	0,0	0,00	SG6042	13	Cosine	19	-Sine
3	1.635,000	260,000	66,000		0,00	SG6042				

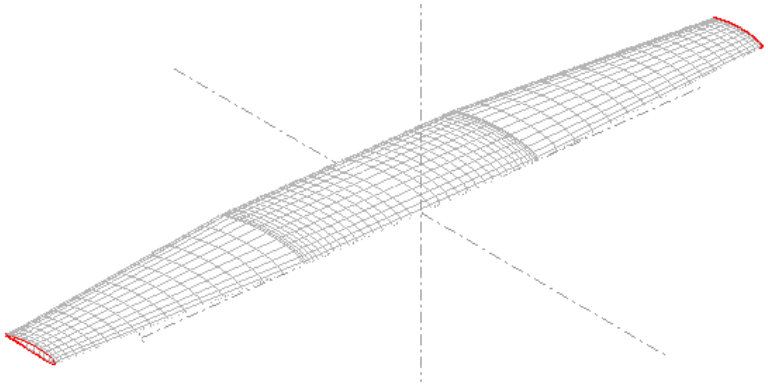

Fig. 30 Wing geometry

Wing area 1.2644m^2; Wing span 3.27m

7.2.3. Tail design

The selected airfoil for both elevator and fin is a symmetrical NACA 0008. The main design criteria to justify this choice is keeping a low relative thickness in order to have low drag but thick enough to contain a rigid CFRP tube. In the case of the fin layout, a trapezoidal planform has been selected to lower the pressure centre keeping the same aerodynamic force but reducing the torsion and bending moment at the attachment point with of the fin with the tail boom. It also helps to obtain a cleaner rudder deflection response by reducing the coupling effect in the roll axis.

	y (mm)	chord (mm)	offset (mm)	dihedral	twist(°)	foil	X-panels	X-dist	Y-panels	Y-dist
1	0,000	330,000	0,000	0,0	0,00	NACA 0008	10	Uniform	15	Cosine
2	300,000	120,000	130,000		0,00	NACA 0008				

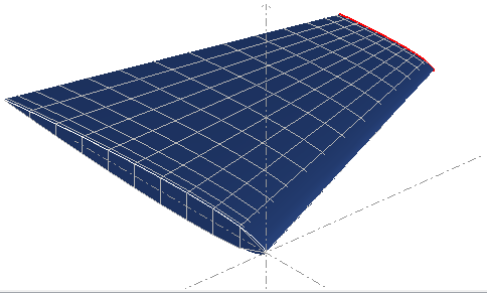

	y (mm)	chord (mm)	offset (mm)	dihedral	twist(°)	foil	X-panels	X-dist	Y-panels	Y-dist
1	0,000	230,000	0,000	0,0	0,00	NACA 0008	11		22	Uniform
2	400,000	140,000	30,000		0,00	NACA 0008				

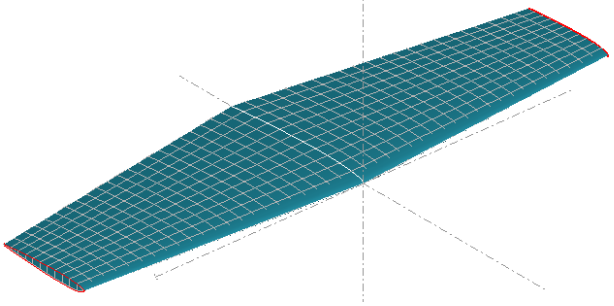

Fig. 31 Tail fin and HTP layout

7.2.4. Static stability

A very critical part of the aircraft design consists of assuring the good natural behavior of the aircraft and pilot-friendliness. Since the regulations do not allow to use electronic aids such as gyros and feedback controlled systems that help to create 'artificial stability'.

Regarding the longitudinal static stability, we have modeled and analyzed in XFLR5 several commercial designs known to fly very stable –such as typical high-wing, 2m wingspan, RC trainers– and found out that most of them have $C_{m\alpha}$ (coefficient of pitching moment) values around -0.025. Ours instead has been set to -0.014 by adjusting tail surface, incidence and distance to wing and CoG position. This setup is marginally less stable but that is a desired result because we really want to trade a bit of static stability by end performance and top speed. Moreover, a neutrally balanced plane has less altitude fluctuations with speed

variation which is also desirable for racing and, in our case, flying the competition legs optimally with less energy waste.

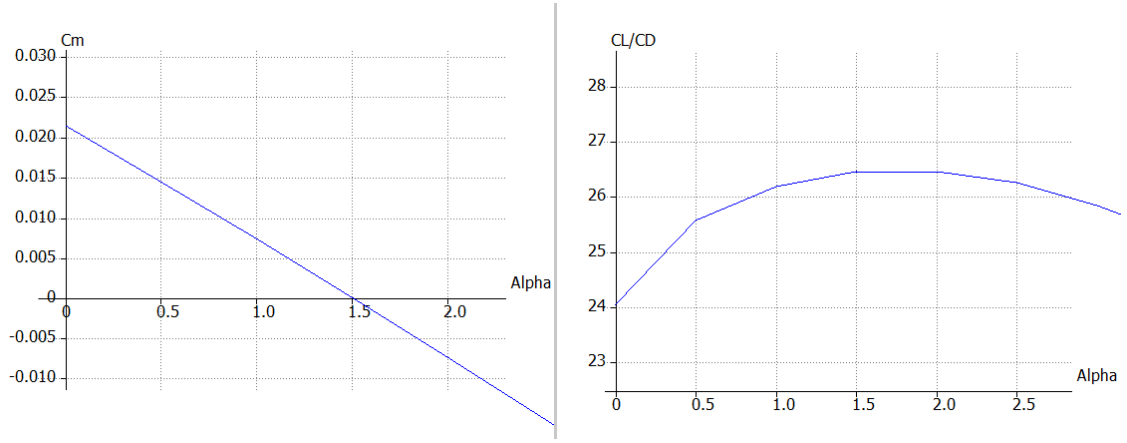

Fig. 32 Cmα-α and CL/CD-α

It can be seen on the above graphs that the coefficient of pitching moment is 0 at 1.5ºAoA, coinciding with the angle of maximum aerodynamic efficiency (E = C_L/C_D) meaning that at this point the airplane does not want to pitch up nor down. If the plane is perturbed and AoA increases, the C_m becomes negative, forcing the plane to nose down again. If conversely, the plane sees a reduction in angle of attack, the C_m becomes positive, making the plane pitch up. That's a natural mechanism to force the plane fly at the desired angle of attack while cruising.

7.2.5. Dynamic stability

On the other hand, we have also studied the dynamic stability of our design by performing a dynamic stability analysis on XFLR5 and examining the obtained poles that represent the natural 'preferred' modes that the airplane adapts in case of wind gusts and other disturbances:

___Longitudinal modes____

Eigenvalue:	-18.12+	-6.649i	-18.12+	6.649i	-0.01095+	-0.5947i	-0.01095+	0.5947i
Eigenvector:	1+	0i	1+	0i	1+	0i	1+	0i
	165.8+	-102.8i	165.8+	102.8i	-0.09216+	-0.003479i	-0.09216+	0.003479i
	-170.6+	4.63i	-170.6+	-4.63i	0.03602+	0.002087i	0.03602+	-0.002087i
	8.214+	-3.269i	8.214+	3.269i	-0.004623+	0.06049i	-0.004623+	-0.06049i

___Lateral modes____

Eigenvalue:	-44.37+	0i	-1.608+	-5.156i	-1.608+	5.156i	0.1246+	0i
Eigenvector:	1+	0i	1+	0i	1+	0i	1+	0i
	52.3+	0i	0.006613+	0.07243i	0.006613+	-0.07243i	0.1204+	0i
	1.958+	0i	0.07917+	0.3074i	0.07917+	-0.3074i	0.5508+	0i
	-1.179+	0i	-0.01317+	-0.002825i	-0.01317+	0.002825i	0.9655+	0i

Fig. 33 Dynamic stability modes

As we can see, all the poles affecting longitudinal stability are located to the left (negative real part) of the complex plane. This implies that the reaction is stable and the natural tendency of the plane in front of disturbances is to correct the deviation in a dampening way. Regarding lateral dynamic stability, again there are negative-real-part poles, which mean disturbances get dampened. There is a positive pole corresponding to the spiral mode which is a non-oscillatory, generally unstable mode that affects heading. It is difficult to neutralize this mode, so the only thing to take into account is to make sure it is low enough so that the deviation is very slow and thus can be easily overcome with small pilot corrections over time. Next we can see an example of the predicted response of our designed aircraft in dutch-roll:

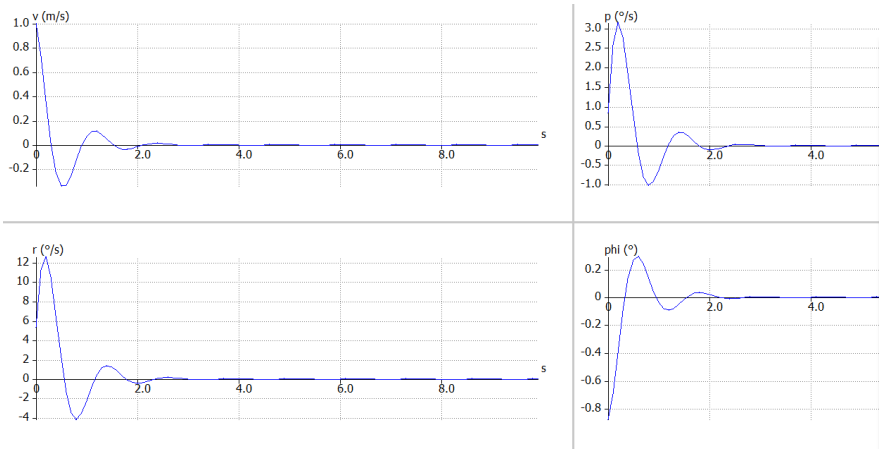

Fig. 34 Dutch-roll dynamic response

The graphs portray the reaction of the aircraft while presented with a rather powerful disturbance that excites the dutch-roll natural mode. Thankfully it gets dampened in about 2 seconds without any need of pilot input.

7.3. Structural and CAD design

When designing the structure of the, it was important to keep in mind that all its components must be able to be transported in a 1100x500x400 mm^3 box. This requirement leads to a wing divided into 3 pieces. Besides, a coupling method is needed.

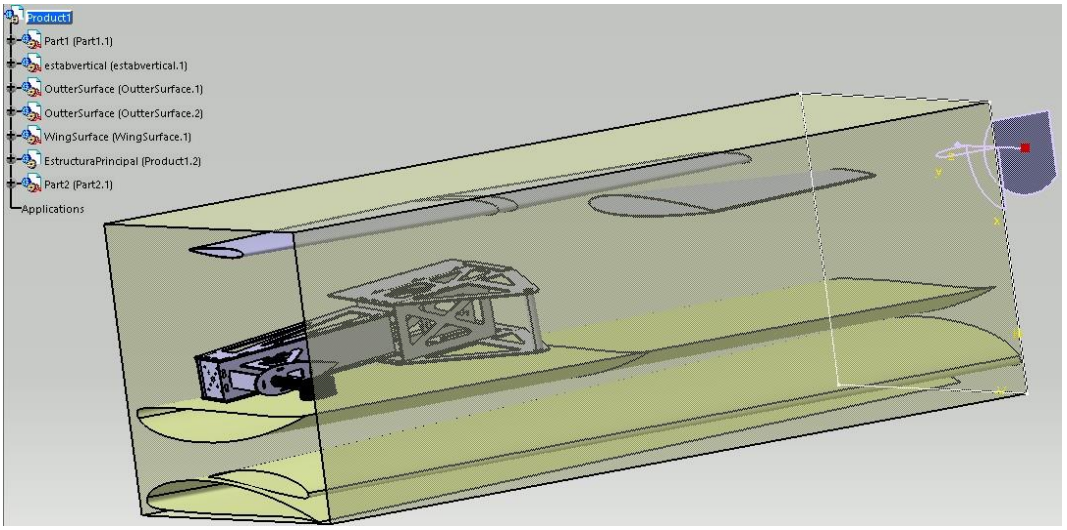

Fig. 35 Transportation box checking

7.3.1. Wing

One of the key points of our design is to restrict the appearance of structure and surface defects to avoid getting a performance lower than predicted. Besides, it is within the scope of this study to make choices based on an analytical approach in order to justify the results rather than designing by trial and error testing.

After considering these options, the CFRP tube has been chosen as main spar. One of the problems found while developing other solutions is that theoretical results would point towards using 'maximum inertia' solutions such as the D-box or torsion box as being more optimal, but the analytic design would be more complex. The CFRP on its behalf, meets our design requirements and fits well our philosophy since it allows an easy wing building process, minimizing assembly tolerance, and analytical stress and strain approximations can be obtained relatively easy. In other cases such as the D-Box, the main problem is not only to avoid component failure caused by the bending moment stresses, but rather predicting and preventing non-linear effects such as local buckling, which requires a substantially more complex mathematical model or designing by trial and error.

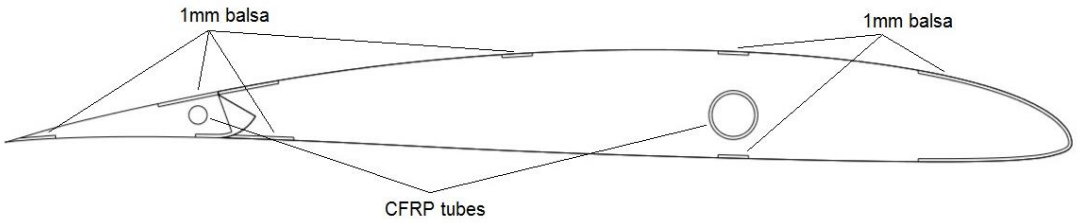

Fig. 36 Wing rib concept

CFRP tube dimensioning has been developed with an Excel worksheet which calculates stresses at different points along the tube assuming that this structure supports on its own the bending moment generated by the wing, earlier calculated with XFLR5. Although other factors could be held into account such as shear stresses, they have been neglected in this first analysis for the following reasons:

- Bending moments are an order of magnitude greater for a structure with such a large span.
- CFRP tube has higher torsion modulus than D-box structure based on the experimental results of UBI team (winner of ACC2011).

Considering these facts, the results include a security factor of SF= 2 for a load factor during turns of load factor n = 2,5. Data obtained from the CFRP

provider sets ultimate strength at up to 1000 MPa during compression, which will be our limit case.

The equations used are the inertia of a cylinder and the maximum compression stress of the fiber located at the top of the tube:

$$\sigma = -\frac{M_y}{I_y} \cdot R_+ \qquad \textit{(Eq. 43)}$$

$$I = \pi\left(\frac{R_+}{2}\right)^4 - \pi\left(\frac{R_-}{2}\right)^4 \qquad \textit{(Eq. 44)}$$

The concept is to use concentric tubes in order to use this main spar as a union for an easy assembly and do not include a redundant structure which would increase weight. Furthermore, this allows to reinforce the root wing spar which withstands a higher bending moment. After dimensioning, the parameters shown in the sketch to the right have been obtained. Outer wing tube thickness is 0.75mm and root tubes are 1mm thickness). The sketch corresponds to half wing. To allow better comprehension, some notes have been added.

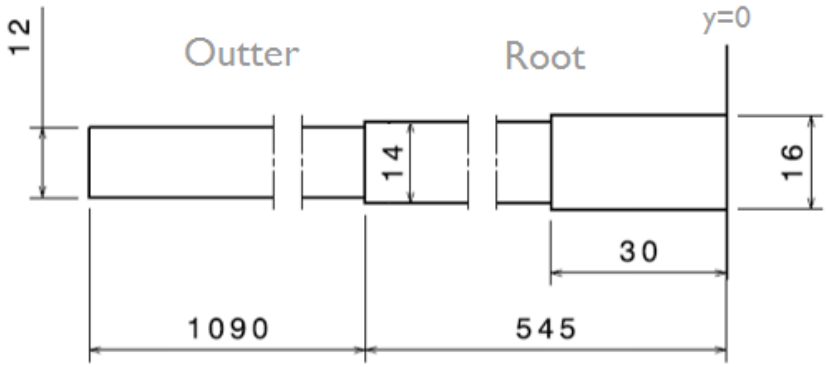

Fig. 37 Wing CFRP tubes geometry

7.3.2. Landing gear and fuselage

Contrary to what one may think, the component that involves a larger number of considerations, hence being iteratively changed during the design process is the landing gear. These were the considerations during its design:

- Stability during take-off
- Contains the cargo bay.
- It has inherently the highest friction term during the runway.
- In our case, connects all the singles structures (wing, tail and engine support).
- Withstands static and dynamic loads.

Due to these requirements, every landing gear concept has many advantages and drawbacks. As the philosophy of the team is described in the report, a conservative attitude has been take unless a significant advantage could be achieved. Thus, it was decided to use a CFRP tube as a common axis that united both wheels. Bearings would be used on each tip to join with the wheel at the lowest friction possible. When aiming for a low friction coefficient between the wheels and the runway we focused on a thin and large wheel and it was not possible find a commercial one that fit the requirements so we proceeded to design one that would. Polyethylene has been chosen as the material due to the easiness of machining the component while being lightweight and still offering a high tenacity that helps absorb the dynamic stresses during landings. Moreover, a rubber band has been included to provide extra cushioning and a thinner contact surface with the ground.

On the nose wheel however, we opted for a commercial trailing link strut leg with spring loaded suspension that already includes a wheel and has very good dampening properties. To provide the pilot with extra control during take-off, the front wheel also includes a servo for steering.

Most of the cargo bay and the motor supporting structure have been made out of plywood and balsa panels with rounded edges in order to reduce stress concentrators and local carbon fiber reinforcements have been added.

This design was chosen because it allows aligning the thrust vector with the center of gravity, which is close to the payload center, reducing pitching moment which makes more difficult for the pilot to stabilize the airplane through elevator tuning. Besides, this concept ensures a nearly perfect aligning of wheels through a carbon shaft, which reduces significantly friction compared to systems where both wheels are not connected.

Since the payload loading procedure time is evaluated for the final score, a quick and reliable way to load the payload into the cargo bay must be engineered. In this regard, the concept design consists of a sliding hatch at the aft of the cargo bay. A portion of the fuselage fairing slides over the tail boom and leaves us with enough space to load up the cargo bay. On the following picture the system is represented (landing gear CAD made by Oleguer Gabernet).

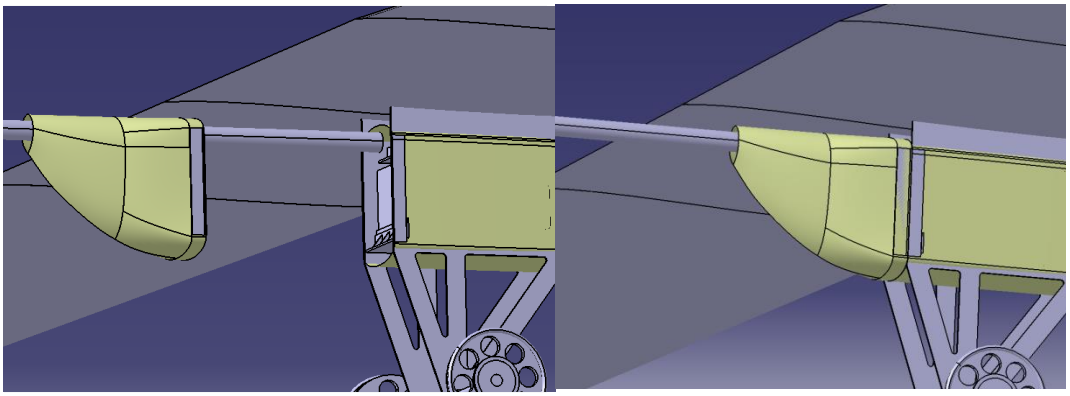

Fig. 38 Fairing hatch system

7.3.3. Tail structure

Regarding the tail, following same procedure to wing design carbon fiber tubes have been used. Moreover, we also added some balsa strips strategically located in order to ease the coating-ironing process of Oracover.

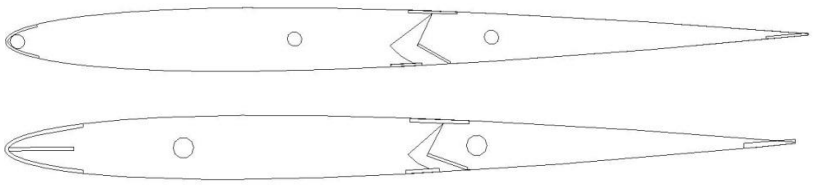

Fig. 39 Fin and HTP rib concepts

7.4. ELECTRONICS

7.4.1. Batteries

Considering the regulations, our battery should be able to deliver more than 45A continuous to avoid overheating.

Batteries chosen are Revolectrix Li-Po battery with specs: 3S 3Ah 40C as main battery to feed the ESC and motor. Maximum discharge rate is calculated as: 40C · 3Ah = 120A >> 45A.

Assuming that we save a 20% capacity on the battery to avoid deterioration of the chemistry. Expected flight time at full throttle is:

$$t = \frac{Battery\ available\ energy}{Discharge\ rate} = \frac{0{,}8 \cdot 3Ah}{45A} = 0{,}05\hat{3}\ h = 3{,}2\ min \qquad \textit{(Eq. 45)}$$

7.4.2. Motor controller-ESC

Same as with the batteries the speed controller has to be able to deal with 45A continuous so we chose a 70A TRUST brushless ESC from Turnigy..

7.4.3. Servos

The servos chosen to actuate the differential ailerons and flaps, the rudder and elevator as well as the wheel steering have been Corona CS-939MG (2,5Kg·cm, 0,14s/60º, 12,5g). These metal gear servos provide high reliability with a low weight penalization. The extra grams are worth since losing a control surface such as the rudder leads to a secure crash.

8. PROPOSED IMPROVEMENTS

After completing the project, the possible changes during the design and manufacturing phases have been studied. In this study, the more important ideas will be explained and the aim is to start the research on every point so that the team can complete this process along the following year.

Regarding recent winning teams, it is a must to include structures with composite skins. To do this, it is needed to acquire the know-how and create sponsor agreements with molding-machining companies. This is a long term task which provides the team the possibility of being competitive if it is combined to the corresponding structural analysis detailed in the following sections.

8.1. Analytic structural spreadsheet

In order to optimize the wing structure and reduce its weight, combining preliminary results from analytic and empirical results with more detailed analysis such as Ansys has to be the path to obtain optimal dimensioning of each component. This analytic method is also important to provide a first order of magnitude of the parameters required for the FEA study.

Applying the theoretical contents presented in 6.3. Structural design, an Excel spreadsheet has been developed importing airfoil geometry, XFLR5 loads and material properties. This Excel calculates stresses in different wing sections. In attachment A.4 the different pages are shown.

After dimensioning a wing box from the 15% chord to the 65%, where usually the aileron is placed, bending moment is withstood by four carbon fiber laminates in the corners, each one having a length of 7 mm. The point of maximum bending moment has been used to this calculus, which is at the root as shown in Fig. 40. These laminates act as cordons of 0,2 mm of thickness. In order to optimize the structure, they could be reduced along the span, but the major part of the wing weight is related to the skin, hence there is no substantial gain.

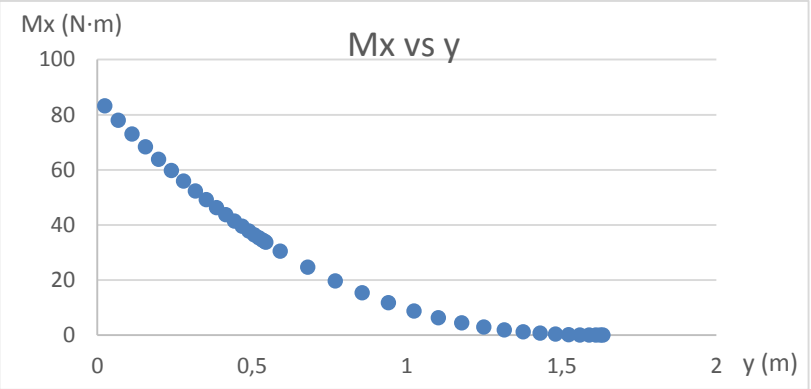

Fig. 40 Bending moment along the span

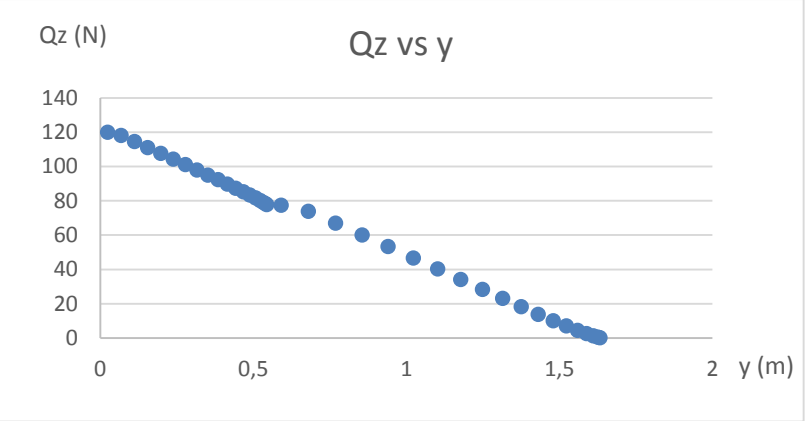

Fig. 41 Shear force along the span

Regarding the shear dimensioning, maximum shear stress was 7,48 MPa for a thickness of 0,05 mm. This value is far from the yield shear strength, which is an order of magnitude higher. Despite this value, the thickness cannot be reduced, therefore it is not overdimensioned.

8.2. FSI study

Fluid-Solid Interaction means coupling the results from the CFD analysis with the mechanical software in order to obtain a distribution of pressure along the surface and design the structure. In this case, the chosen software has been Fluent for the flow study and Ansys Mechanical for the structural part. This method allows to obtain a realistic distribution of loads (not only bending moment as it has been considered previously) and CFD analysis could provide more accurate data than XFLR5.

8.2.1. Fluent

CFD software solves the coupled equations mentioned in 6.1.1. based on different hypothesis of the wall function, which determines the boundary layer behavior, hence being a powerful tool. However, for the preliminary design and first parameters calculations, CFD is not viable since creating an acceptable mesh is a time-consuming task and every analysis requires from half an hour in simple models to 5 hours of computational processing. Since optimizing the 3D mesh and validating results completing a full CFD study could standalone as a TFG, the scope of this study is to obtain approximate results and show the advantages of the process of transferring pressure distribution to structural module, beyond fulfilling formal aspects of validation and improving the mesh in terms of computational cost.

Before starting, Ansys Workbench interface has to be introduced. On the left menu, pick a Fluent component. This module has different sections: geometry, mesh, setup and results. The procedure and considerations of each one will be detailed:

Geometry

First of all, it is required to create a control volume for the fluid domain and the wing surface itself. In this case, both have been imported from Catia. Since the control volume to be meshed is a solid, previously the wing surface must be converted to solid (Create- Body operation- Sew) and then be subtracted (Create- Boolean). Moreover, it is useful to create Named Selections for the different faces of the fluid domain, since they establish the boundary conditions.

Mesh

This part is the most critical when studying flow over any kind of surface in order to obtain realistic results. In this case, unstructured grid with global and local algorithms included in the software have been used with automatic blocking. For a further optimization of the mesh, blocking should be modified manually using

another specific module such as ICEM-CFD. One must notice that refining the mesh increases the number of cells, hence increasing the computational time per analysis and memory required. In this computer, the limit of 8GB was reached about 4.000.000 cells. After iterating by trial and error, the first successful mesh to be validated presented 3.083.028 cells.

Among the global algorithms, advanced size function has been set on proximity and curvature including some restrictions to improve mesh quality such as curvature normal angles limited to 10º. Regarding at local algorithms, face sizing provides detail of the evolution of the gradient in *x* and *y* local directions, with a limited element size of 1 cm and curvature normal angle of 5º. Meanwhile, inflation provides extra refining on *z* direction in order to analyze the boundary layer.

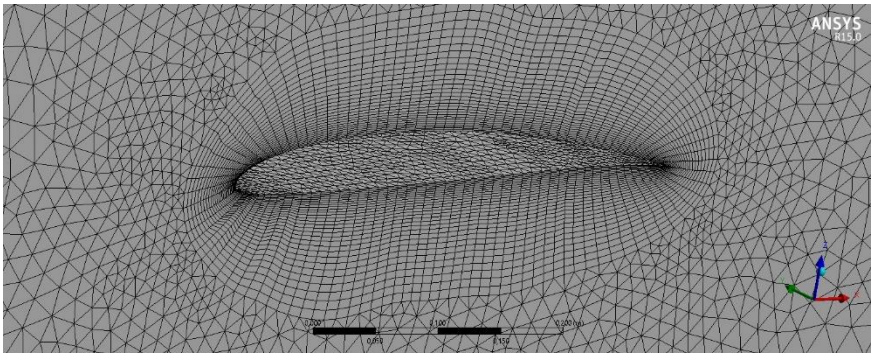

Fig. 42 Fluent mesh detail

In order to evaluate the quality of the mesh, following the recommendations of the Cornell University, it has been checked than the minimum orthogonality is >0.15, maximum skewness <0.95 and the average values of those compared to the following table give an estimation of the quality. In this mesh, minimum orthogonality is 0.102, maximum skewness is on the limit (0.952), but the average stands as outstanding (0.239). These results are justified with a coarse mesh far from the surface to keep the number of cells under 4.000.000, but the average quality near the airfoil, where most of the cells are placed, is acceptable.

Skewness:

Outstanding	Very Good	Good	Sufficient	Bad	Inappropriate
0-0.25	0.25-0.50	0.50-0.80	0.80-0.95	0.95-0.98	0.98-1.00

Orthogonal quality:

Inappropriate	Bad	Sufficient	Good	Very Good	Outstanding
0-0.001	0.001-0.15	0.15-0.20	0.20-0.70	0.70-0.95	0.95-1.00

Table 2. Mesh quality values
Cornell University, https://confluence.cornell.edu/pages/viewpage.action?pageId=262012971 (accessed 14 September, 2015)

Setup

In order to solve the different parameters of each cell, Fluent provides different models of analysis. When studying a low Reynolds wing case, it must be pointed out that phenomena associated to the boundary layer are more complex than a civil aircraft wing. Since most of the industrial cases are fully turbulent, the standard k-ε model works accurately. However, in low Reynolds two characteristic phenomena can occur. First of all, when critical Reynolds number reached, there is a transition from laminar to turbulent flow which is difficult for the software to predict. Besides, when reaching high angles of attack near the stall, a boundary layer detachment can appear, which significantly changes the behavior of the fluid since it becomes really transient. In fact, the solvers used are RANS based, which means they work with average values in order to obtain steady values.

The models considered ones for this case have been following CFD experts' advice in specialized forums such as cfd-online.com and literature with experimental data. These are: Spalart-Allmaras (1 equation), intended to solve simple geometries in aerospace sector such as airfoils and wings, SST k-ω (4 equations) and the Reynolds Stress Model (7 equations). Intuitively, more equations lead to higher accuracy but higher computational cost as well.

Results

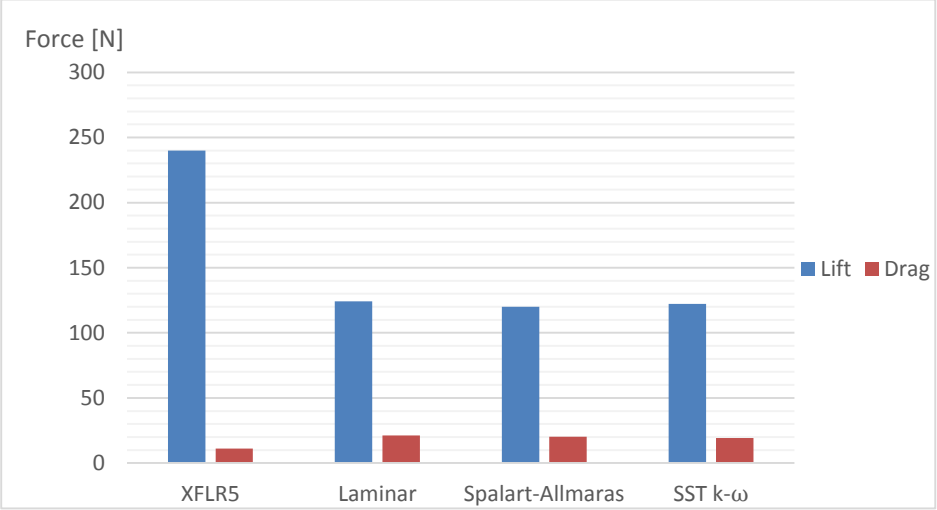

Fig. 43 Lift and drag comparison between XFLR5 and Fluent

Conditions of analysis are v=18 m/s and α=7º, which correspond to the limit case with n= 2,5 during turns. These results are obviously far from reality. In order to study the cause, different plots have been studied. Pressure contours in all methods provide a realistic distribution along the surface, despite of not showing any detachment of the boundary layer. It has been represented as well the pressure distribution in a plane to see 2D pressure in the flow domain, located at 0.2m from the root (Fig. 45).

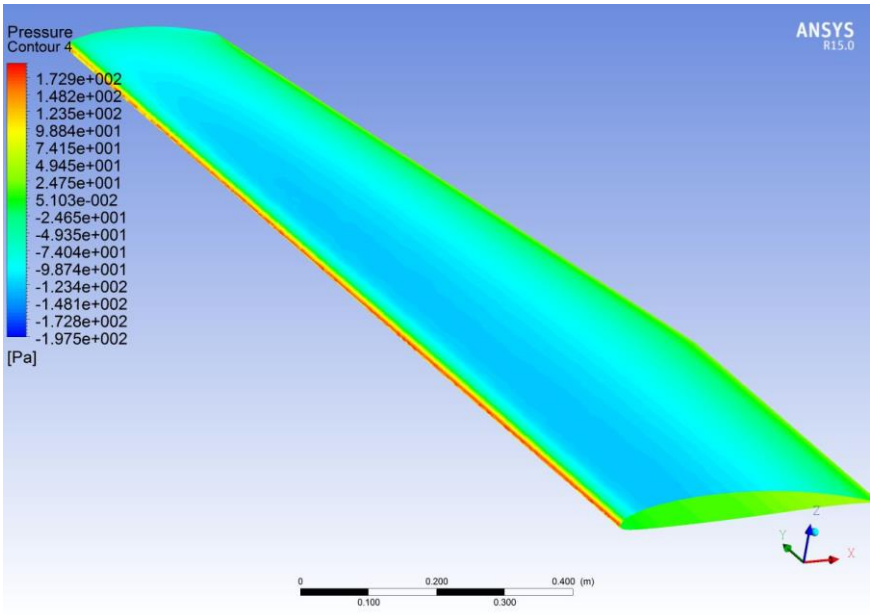

Fig. 44 Pressure contour along the wing

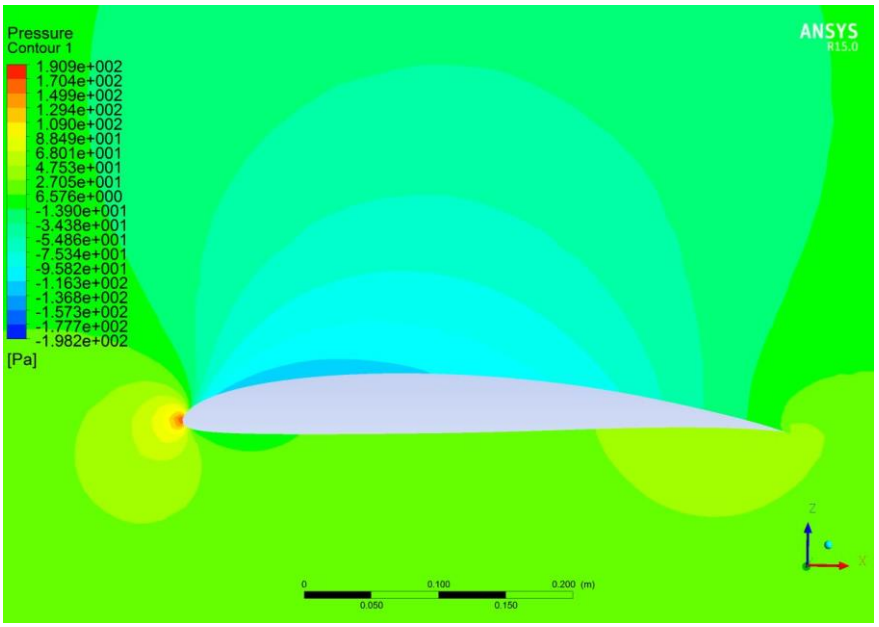

Fig. 45 2D pressure distribution

In order to analyze these results and the cause of not matching with the XFLR5 predictions, an additional contour has been represented showing turbulence kinetic energy along this section (Fig. 46). This analysis shows that the software is applying a transition since the turbulent boundary grows along the chord. The problem is that probably with this mesh or these model parameters the software is not able to predict the correct distribution of pressure since there should appear a negative gradient of pressure in the rear part of the airfoil.

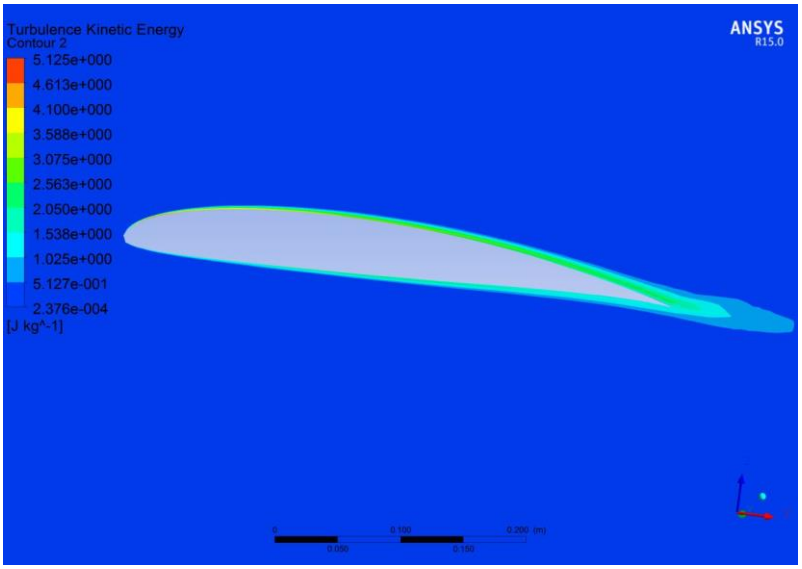

Fig. 46 Turbulence kinetic energy 2D plot

8.2.2. Ansys Static Structural

As the results of the CFD analysis did not match the real distribution, this part of the study just intends to show up the methodology of coupling this distribution to the structural module.

Ansys provides a very easy use of this coupling. It is only needed to slide the CFD Results component in Workbench to the structural Setup and import loads inside it.

To enhance the parameterization the structure, Catia surface has been divided by the torsion box surfaces (leading edge, trailing edge, wing box skins, front beam and rear beam) for both root and outter part. This method allows to set different thicknesses for every surface in order to optimize the structure.

Concerning the mesh generation, inside the Setup part it is possible to set the Face sizing. By default, when importing a surface geometry the solver uses Shell 181 elements. These shells are useful when working on geometries with two reference lengths larger than the other (which is our case, where thickness of the walls is four order of magnitude lower than chord and five compared to span).

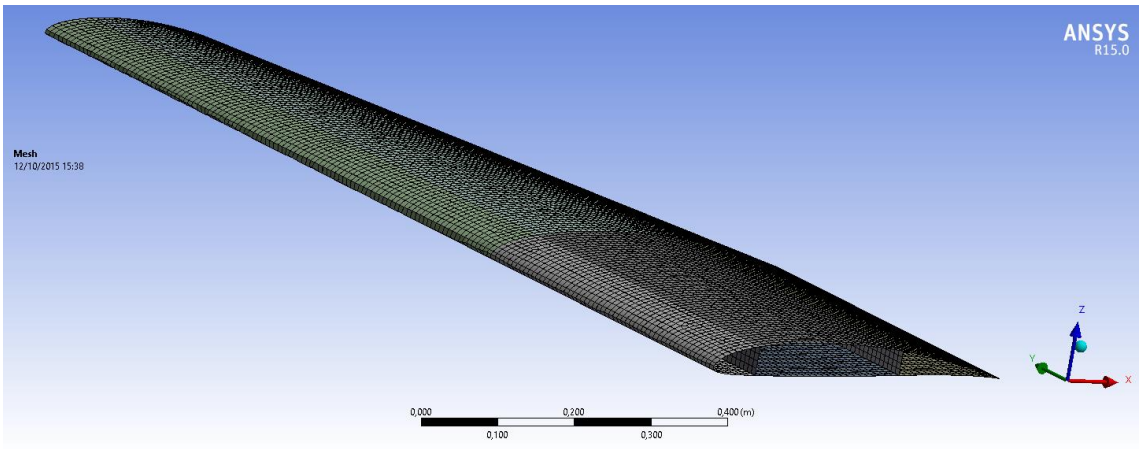

Fig. 47 Wing mesh in Ansys

As a qualitative idea, the results that can be obtained from the analysis are shown below. Despite of not being rigorous, since the CFD analysis was already far from reality, they have been included to show the capabilities of the FSI study.

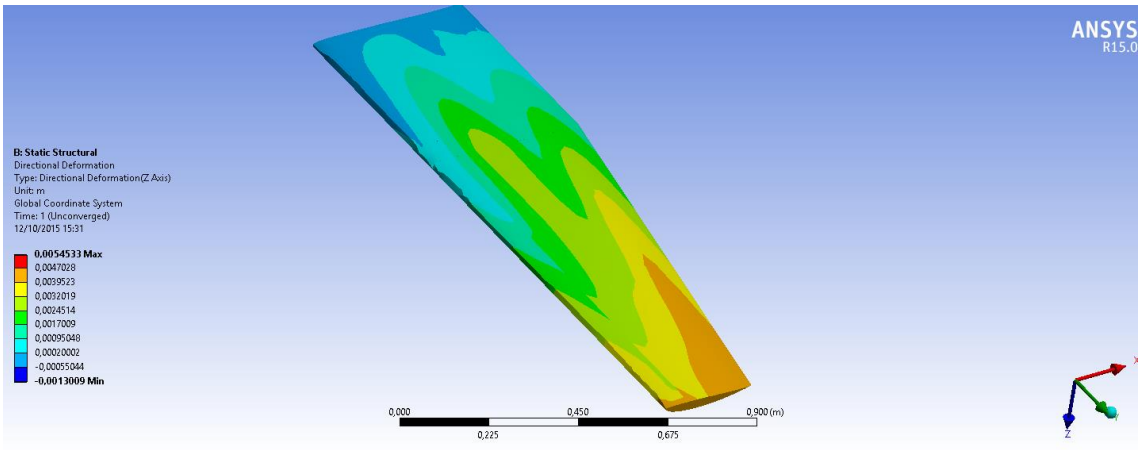

Fig. 48 Vertical displacements of the wing in Ansys

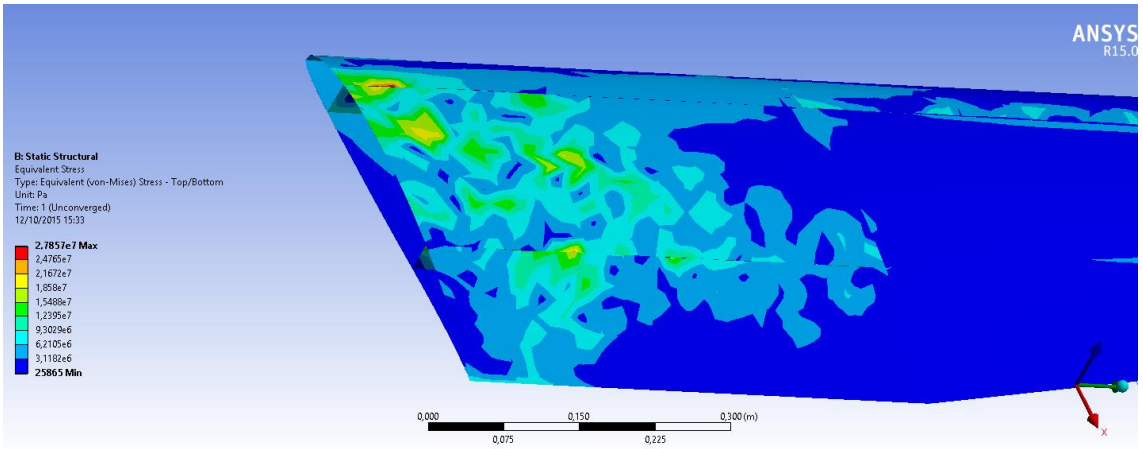

Fig. 49 Von-Mises stresses of the wing in Ansys

8.3. Semi-analytical thrust prediction

In order to have reliable data from the thrust-speed curves, experimental sources (when the measurement errors are reduced) are always the best source of information. As it has been mentioned earlier in 6.2, analytical predictions fail to predict static thrust due to non-ideal behavior.

Nevertheless, before studying our propulsive system with a benchmark, it would be necessary a method to choose between different motors, propellers and batteries. In the case of a competition as the ACC usually engine is fixed, but every propeller gives a different performance. If there were not requirements concerning this aspect, for example building a UAV for civil purposes, a criterion to choose the optimal configuration is needed. To solve this problem, using data provided from the manufacturer and other coefficients as inputs, a software called MotoCalc obtains the thrust vs speed curves (it is not open-source, but it offers 30 days trial). This way, it is possible to export the results to the Matlab codes and treat the propulsive system as another variable known.

The graph below (Fig. 50) shows a comparison between the experimental data from the study mention in 6.2 and the results of MotoCalc. As expected, the static thrust is overestimated in the semi-analytical method. However, for higher speeds opposite phenomena occurs. However, this tool allows acquiring qualitative data. For example, using13x7 propeller instead of 13x6,5 would allow higher cruise speed. This data should be useful for a preliminary model of engine and propeller selection.

Concerning quantitative analysis, this method is not really accurate (error oscillates between 18%, in the case of static thrust, and 30%). It must be reminded that this is external data and it is not ensured that the experimental measurements are correct. Moreover, the batteries used are not specified, whose voltage is relevant. Therefore, comparing and validating the different models with a propulsive benchmark should be considered in the development phase until next edition.

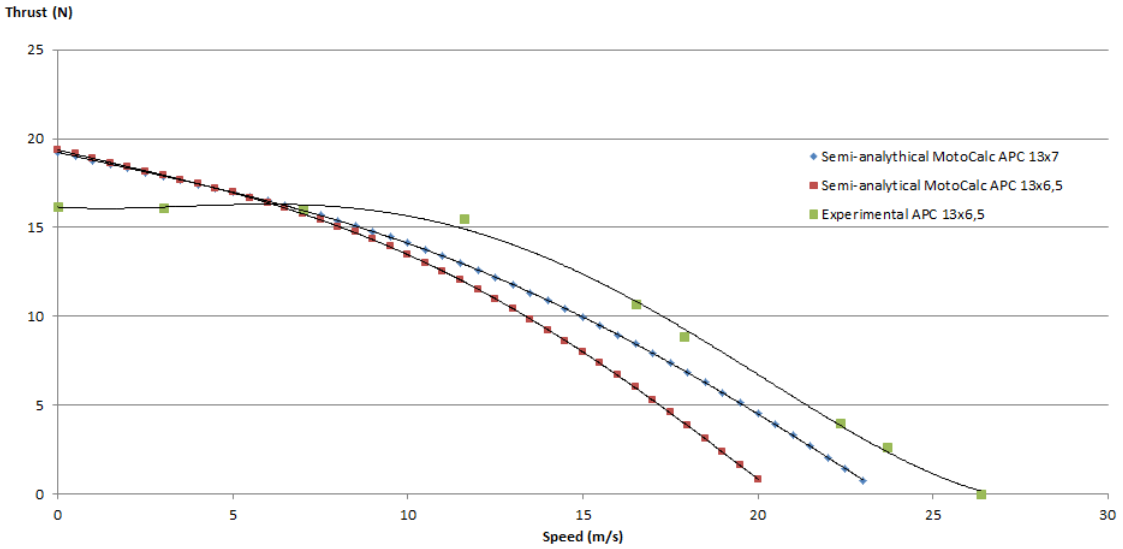

Fig. 50 Thrust analysis method comparison

8.4. Friction coefficient characterization

During take-off first meters, ground friction is a bigger term than aerodynamic drag. The characterization of this value will provide important data to a better prediction model. One of the problems of the landing gear friction model is that may not be linear, since loading higher payload leads to a shaft deflection and tires contact angle vary, increasing friction.

To solve this problem, a typical experiment applying second Newton's law (Eq. 46) to acquire kinetic friction data is represented in the sketch below.

$$\sum F_x = T - F_r - F_f = ma_x \qquad \textit{(Eq. 46)}$$

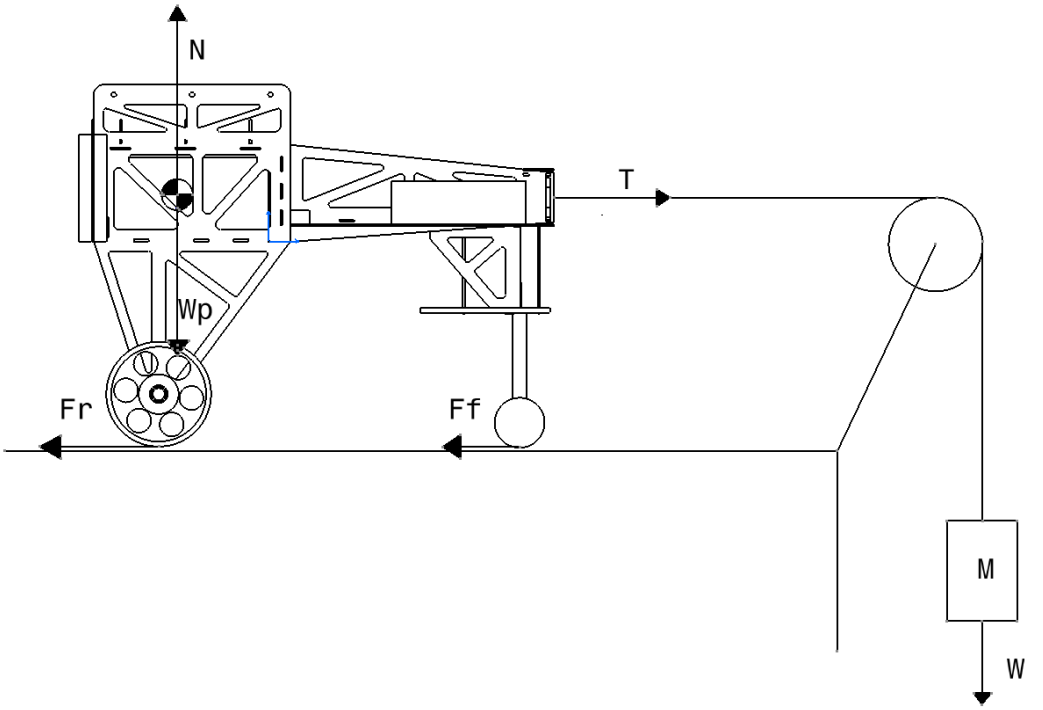

Fig. 51 Landing gear forces diagram

Tension equilibrium provides $T = W$ and the aim is to increase weight until the landing gear slightly moves with $a_x = 0$ condition. Applying equilibrium in y direction, $W_p = N$ and manipulating terms, the following equation is obtained.

$$W = F_r + F_f = \mu_k N = \mu_k W_p \qquad \textit{(Eq. 47)}$$

Representing W vs W_p with the experimental data varying payload ($W_p = TOW + PL$) , it is possible to calculate a regression for the friction kinematic coefficient, hence providing the value of this coefficient during preliminary design depending on the MTOW.

9. ECONOMIC SUMMARY

To sum up the treasury statement of the project, the incomes (Table 3) and the budget (**¡Error! No se encuentra el origen de la referencia.**) are detailed below. The main difficulty to face along the development of the project has been the lack of liquidity, from a cash-flow analysis, these incomes coming from public grants are received after the bills are justified. This meant that team members had to lend most part of the capital in advance to complete the project. For further information, check the Budget document.

INCOMES	
INSPIRE3	2.000
AJUNTAMENT TERRASSA	1.170
CONSELL DE L'ESTUDIANTAT UPC	495,29
TOTAL	3.665,29

Table 3. Incomes

EXPENSES			
Name	**Units**	**Price/unit**	**Total (€)**
Competition			
ACC2015 registrations (7 members)	7	180	1.260
Flight tickets (7 PAX)+ Transportation box			930
Materials and tools			
Dremel 3000	1	69,55	69,55
Manual tools			100
TeXtreme carbon fiber			0
Bearings	8	2	16
Fairing materials JePe			63,69
Adhesives			30
Composite materials R&G			433,77
Auxiliar workshop tools			50
Aeromodel woods R. Agulló			286,98
Electric systems			
Motor and propeller RC Madrid			119,28
Batteries 3000mAh Revolectrix	3	21,94	65,82
Transport taxes Revolectrix			14,8
Electronics RC Tècnic			148,15
Electronics HobbyKing			77,69
External tooling			
Wood laser cutting *Laser Project*			0
Wheels mechanizing *Dovan*			0
TOTAL			3.665,73

Table 4. Budget

10. ENVIRONMENTAL IMPACT

Considering the design phase, using computer-aided tools has required a huge amount of engineering hours by all team members. As an estimation, every member spent 20h analyzing aerodynamic configurations, 300h were spent in generating geometry in Catia and 100h generating reports and documents for subsidies. An average 400W is considered for these computers since it is needed a high percentage of CPU capacity.

During the last month of manufacturing and assembly, Dremel tool was used constantly to do polishing, drilling, make holes... As an estimation it will be considered that it was used 3h every day during 20 days with an average power of 60W (despite having 120W nominal power, this can be regulated by the operator).

About laser cutting energy required, Epilog Fusion 32 M2 machine was used, which consumes from 30 to 120W. In our case, balsa and plywood cutting requires low energy compared to other materials such as aluminum or steel plates, so 30W are considered. Around 10h of cutting time were necessary.

Besides, the CO2 emissions during our roundtrip flight to Stuttgart must be considered. For seven passengers, they are estimated to be 1,16 tones.

Process	Energy [kWh]
Computer design	216
Dremel tooling	3,6
Laser cutting	0,3
Process	CO2 emissions [tones]
Flights	1,16

Table 5. Summary of environmental impact

As a positive aspect, it must be pointed out that the use of these computational tools reduce the number of experimental tests, hence there is low waste of materials.

11. SAFETY CONSIDERATIONS

During the manufacturing phase there are several important points regarding safety and health considerations. Since team members are working in a reduced place with low air circulation, especial attention must be put into tasks where chemical components and volatile particles are produced, which are hazardous when breathed. To prevent these effects, always use high quality masks, lab coats and latex or similar gloves, avoiding direct contact with chemical components.

When manipulating carbon fibers pay extra attention to avoid body contact, since it causes skin irritancy. There are other chemicals such as epoxy resins where the harmful pictogram is found. Due to recent change in the law chemical classification and labelling, both old and new symbols are shown:

1. Explosive
2. Oxidising
3. highly flammable
4. Toxic
5. Harmful
6. Irritant
7. Dangerous for the environment

Fig. 52 CLP pictograms
(Health and Safety Executive n.d.)

Regarding at the propulsive system, the following practices must be had into account to ensure total safety during operation of the electric engine:

- Use tools and equipment with non-conducting handles when working on electrical devices, disconnecting batteries before manipulating engine circuit.
- Before connecting the transmitter, make sure the propeller is fixed to the engine and never stand in front of it. Propeller has a sharped shape and it is rotating at 8.000 – 15.000 rpm. Make sure people near the area is behind the plane.

12. FUTURE TASKS PLANNING

In order to achieve the improvements recommended, there are three work lines: the prediction section, the FSI study and the manufacturing technique.

The prediction section includes acquiring more accuracy in the parameters involved in the preliminary design codes. The aim is to complete these points:

- Validate the hypothesis made, which have worked and which not compared to the other teams results.
- Building a propulsion benchmark and complete experimental data acquisition. Compare the measurements to analytical data.
- Building the friction coefficient benchmark and complete experimental data acquisition. Compare the range of values from the measurements with similar materials coefficients.
- Test materials experimental properties.

The FSI study will complete the detailed engineering phase. The aim is to complete these points:

- Improve CFD results using ICEM-CFD through manual blocking to optimize the mesh with hexa structured grid. Compare the results with XFL5.
- Complete the mechanical simulation with buckling module. Include core materials in sandwich structures and vary its thickness.

Finally, to achieve an optimal manufacturing know-how, it is required to test several samples. The following steps are needed:

- Research on molding materials for our application and geometry issues.
- Create the CAD files and manufacture them in external companies.
- Build the samples and do structural tests varying resin proportions.

Task name	Duration
Prediction	
Teams benchmarking	6 days
Build propulsion benchmark	15 days
Validate prediction code	10 days
Build friction benchmark	5 days
Material experimental test	4 days
FSI study	
CFD mesh refinement	10 days
Static mechanical FEA	5 days
Buckling FEA	10 days
Manufacturing	
Mold materials	5 days
CAD molds	5 days
Molds manufacturing	5 days
Laminate samples	10 days
Structural tests	5 days

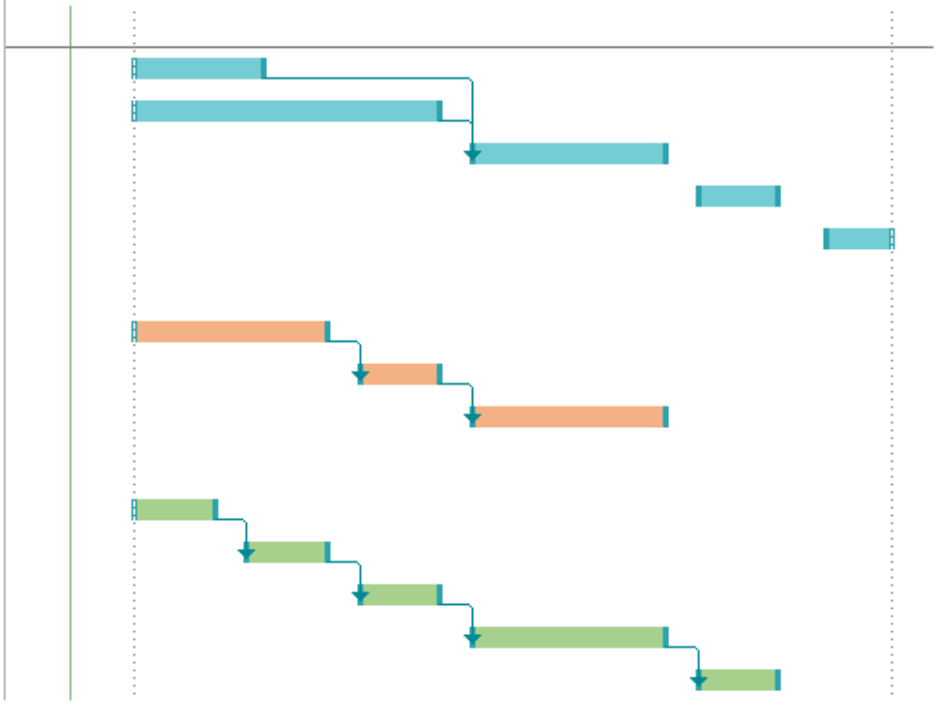

Fig. 53 Future tasks planning

13. CONCLUSIONS

The creation of UPC Venturi and development of this project has been an intense experience for all the team members. Despite the difficulties of having limited resources and short experience, the team has achieved a 10th position out of 29 international participants carrying a payload of 5.1kg, which is the best score so far for our university.

Regarding at the technical aspects, the overall performance of the aircraft in terms of stability and control was positive. Moreover, the take-off payload predictions were successful, lifting 7,5kg in our last round despite of not being able to complete the flight pattern. Moreover, the winning team selected the same concept design, a conventional aircraft with T-tail, which validates our process. However, there have been some differences between the first teams and our proposal as it has been mentioned before. The semi-monocoque structure and the corrections in the score prediction could have been substantial improvements. The design tools developed during this study hopefully will be the seed of an optimization process for the following editions, especially concerning structural dimensioning. Furthermore, the application of these tools would be suitable for any kind of projects the team decided to start.

In relation to the main difficulties shown along the project, they can been divided in technical and management ones. Considering the technical field, whichever is the next project, obtaining experimental data from the propulsive system is critical. It would have been a complex issue to solve as developing an engine bench is a project itself and we would not have had enough time to complete it. In this line, the analytical method will provide a first approach during preliminary design. Furthermore, the lack of resources for mold mechanizing did not allow to the optimal structures.

In the case of management issues, one of the main problems has been acquiring liquidity since most of the cash was advanced by team members until subsidies were granted. One of the proposed solutions would be creating a crowdfunding campaign.

Concerning the planning and scheduling of the tasks, despite of cancelling some weeks due to exams, during the development of the project it has been difficult to combine lectures, deliverables and the tasks assigned. Not having full availability of the human resources has led to some delays. Nevertheless, the team has met the deadlines such as the final report hangout and these delays have not been accumulated. It is true, though, that these deadlines have caused important picks of work. For future projects, it could be positive to communicate availability prior to the project manager, allowing a better management of the human resources and scheduling.

At a personal level, demonstrating interest on the aerospace field through the participation of this non-profit projects developed by students can provide a junior profile to stand out of the rest. In my case, it has been one of the main topics of discussion during interviews since recruiters are very interested in knowing in detail which are the teamwork dynamics and the activities that provide extra value, such as being in charge of a sponsor relationship or managing requirements and deadlines. Since one of the main problems of graduate students is the lack of practical experience, participating in these kind of projects not only shows motivation and proactivity, but a first contact with the industrial sector.

Fig. 54 V-15 in Stuttgart

14. BIBLIOGRAPHY

Andersen, L., Nielsen, S.R.K.. *Elastic Beams in Three Dimensions*. Available at: http://homes.civil.aau.dk/jc/FemteSemester/Beams3D.pdf [Accessed May 5, 2015].

Anderson, J.D., 1991. *Fundamentals of Aerodynamics.* 2nd ed. I. McGraw-Hill, ed., New York.

Anderson, J.D., 2005. *Introduction to Flight.* 3rd ed. I. McGraw-Hill, ed., Boston.

Bruhn, E. & Bollard, R., 1973. *Analysis and design of flight vehicle structures.* Ed. S.R. Jacobs.

De Resende, O.C., 2004. *The Evolution of the Aerodynamic Design Tools and Transport Aircraft Wings at Embraer*. J. of the Braz. Soc. of Mech. Sci. & Eng.

Eastern Michigan University. *Experiment #13 Kinetic friction*. http://www.emich.edu/physicsastronomy/facilities/course_labs/sample_report_long.pdf [Accessed September 25, 2015].

Euroavia Stuttgart, 2014. *Regulations for the Air Cargo Challenge 2015*. Stuttgart.

Health and Safety Executive, *Hazard symbols and hazard pictograms*. Available at: http://www.hse.gov.uk/chemical-classification/labelling-packaging/hazard-symbols-hazard-pictograms.htm [Accessed May 10, 2015].

Lozano, P., 2008. *Fluids – Lecture 9 Notes*. Available at: http://web.mit.edu/16.unified/www/FALL/fluids/Lectures/f09.pdf [Accessed April 17, 2015].

NASA, Parts of an aircraft: Wing design. Available at: *http://www.aeronautics.nasa.gov/pdf/wing_design_k-12.pdf [Accessed May 2, 2015].*

Niu, M.C.-Y., 1988. *Airframe Structural Design*. Conmilit Press, Ltd. Wanchai.

Project Management Institute Inc., 2000. *A guide to the project management body of knowledge (PMBOK® guide)*. PMI publications, Pennsylvania.

Roskam, J., 1985. *Airplane Design Part I - Preliminary Sizing of Airplanes* DAR Corporation, ed., Lawrence KS, USA.

SAE R-424, 2010. *Composite Materials Handbook (CMH-17) Volume 3, Polymer Matrix Composites: Materials Usage, Design, and Analysis*. SAE International.

Toreenbek, E., 1986. *Synthesis of Subsonic Airplane Design.* 3rd ed. Delft University Press, ed., Martinus Nijhoff Publishers.

Software used:

Ansys Workbench v15.0
Catia V5
Microsoft Project
Microsoft Office
MotoCalc v8.0
SmartDraw CI
XFLR5 v6.11